Atmos. Meas. Tech. Discuss., 5, 4195–4247, 2012
www.atmos-meas-tech-discuss.net/5/4195/2012/
doi:10.5194/amtd-5-4195-2012

Atmospheric Measurement Techniques Discussions

Retrieval interval mapping, a tool to optimize the spectral retrieval range in differential optical absorption spectroscopy

L. Vogel[1], **H. Sihler**[1,2], **J. Lampel**[1], **T. Wagner**[2], **and U. Platt**[1]

[1]Institute of Environmental Physics, University of Heidelberg, Im Neuenheimer Feld 229, 69120 Heidelberg, Germany
[2]Max Planck Institute for Chemistry, Hahn-Mertner-Weg 1, 55128 Mainz, Germany

Received: 15 March 2012 – Accepted: 30 May 2012 – Published: 13 June 2012

Correspondence to: L. Vogel (leif.vogel@iup.uni-heidelberg.de) and
H. Sihler (holger.sihler@iup.uni-heidelberg.de)

Published by Copernicus Publications on behalf of the European Geosciences Union.

Abstract

Remote sensing via differential optical absorption spectroscopy (DOAS) has become a standard technique to identify and quantify trace gases in the atmosphere. The technique is applied in a variety of configurations, commonly classified into active and passive instruments using artificial and natural light sources, respectively. Platforms range from ground based to satellite instruments and trace-gases are studied in all kinds of different environments. Due to the wide range of measurement conditions, atmospheric compositions and instruments used, a specific challenge of a DOAS retrieval is to optimize the parameters for each specific case and particular trace gas of interest. This becomes especially important when measuring close to the detection limit.

A well chosen evaluation wavelength range is crucial to the DOAS technique. It should encompass strong absorption bands of the trace gas of interest in order to maximize the sensitivity of the retrieval, while at the same time minimizing absorption structures of other trace gases and thus potential interferences. Also, instrumental limitations and wavelength depending sources of errors (e.g. insufficient corrections for the Ring effect and cross correlations between trace gas cross sections) need to be taken into account. Most often, not all of these requirements can be fulfilled simultaneously and a compromise needs to be found depending on the conditions at hand.

Although for many trace gases the overall dependence of common DOAS retrieval on the evaluation wavelength interval is known, a systematic approach to find the optimal retrieval wavelength range and qualitative assessment is missing. Here we present a novel tool to determine the optimal evaluation wavelength range. It is based on mapping retrieved values in the retrieval wavelength space and thus visualize the consequence of different choices of retrieval spectral ranges, e.g. caused by slightly erroneous absorption cross sections, cross correlations and instrumental features.

The technique is demonstrated using the examples of a theoretical study of BrO retrievals for stratospheric BrO measurements and for BrO measurements in volcanic

AMTD

5, 4195–4247, 2012

plumes. However, due to the general nature of the tool, it is applicable to any type (active or passive) of DOAS retrieval.

1 Introduction

Differential optical absorption spectroscopy (DOAS) is an established technique to quantify the concentration and distribution of a large number of atmospheric gases in the ultraviolet (UV), visible (VIS) and near-infrared (NIR) wavelength ranges (Platt and Stutz, 2008). The technique is based on the Lambert-Beer-law (also known as Bouguer–Lambert-law), which states that the intensity of electromagnetic radiation with an initial intensity I_0 will decrease exponentially depending on the amount of absorber present and its respective absorption cross section. The idea behind DOAS is to split the absorption cross section $\sigma(\lambda)$ in its broad band and narrow band parts (absorption structures widths typically smaller than a few nm). This narrow band part is also called the differential absorption. Thus it is possible to determine the amount of a trace gases with sufficiently strong differential absorption features by splitting the total absorption into broad band extinction and narrow band absorption. A suitable filter, e.g. a polynomial can be applied to describe the combined broad absorption structures together with Rayleigh and Mie extinction and broad band instrumental features, whereas the amount of trace gases of interest are derived from their narrow band absorption structures. Due to the differences in differential absorption structures, it is possible to retrieve different trace gases in the same measurement and spectral region. In this case, the intensities recorded need to be carefully separated in order to determine the integrated concentration of the trace gases along the light path, the slant column density (SCD). In many scenarios, the absorption of the trace gas of interest is concealed by stronger absorbers present. Small errors in reference absorption cross sections (RCSs) might lead to small errors in determination of the strong absorber, but can heavily influence the retrieval results of other much weaker absorbers.

AMTD
5, 4195–4247, 2012

DOAS instruments can be classified into active and passive DOAS instruments, which apply artificial light sources natural light sources (scattered sun, direct sun, moon or star light), respectively. Active DOAS instruments allow to compare spectra of light before and after a beam has passes a known distance through a volume of air containing the absorbing gas. For practical purposes, long-path instruments (LP-DOAS) are limited to measurements near the ground due to the necessity of stable deployment of light source, receiver as well additional reflectors (e.g. Merten et al., 2011, and references therein). This may not be necessary for Cavity-Enhanced DOAS (CE-DOAS) (e.g. Platt et al., 2009). Passive instruments use natural light sources. This allows for the construction of versatile instruments which are compact and of low power consumption without necessities for an additional emitter and reflectors. Applications include satellite measurements and Multi-AXis DOAS (MAX-DOAS) from different platforms (ground based, aircraft, balloon and ships), car traverses, which have been applied to a multitude of scientific problems including measurements of volcanic plumes.

For a comprehensive overview over different DOAS systems and the evaluation technique see Platt and Stutz (2008).

The wavelength interval in which the DOAS retrieval is performed is one of the most important parameters of the retrieval process. Obviously, the interval should include prominent absorption features of the trace gas of interest in order to obtain optimum sensitivity, whilst excluding strong absorptions features of other trace gases and possible instrumental artefacts. Thus, a balance has to be found between sensitivity and possible interference. A broader interval increases the information available to the algorithm, but also involves the danger of incorporating strong absorption structures of other gases present. In some cases, a broader wavelength range can increase errors e.g. due to insufficient correction of the broad band terms (Marquard et al., 2000; Pukite et al., 2010). Other effects to be considered are the wavelength dependency of the Ring effect at presence of higher aerosol loads or clouds (e.g. Wagner et al., 2009, and references therein) and radiative transfer effects when measuring volcanic plumes (Kern et al., 2010). A narrower evaluation wavelength range on the other hand

AMTD
5, 4195–4247, 2012

can lead to an increase in cross correlation between the different RCS, moreover the retrieval might be more strongly influenced by the DOAS high-pass filtering (e.g. fitting of a polynomial).

Despite the importance of the problem only few attempts were made to systematically and quantitatively assess the influence of the retrieval wavelength range on the resulting SCDs. In most publications, the applied retrieval wavelength ranges are only motivated by a comparison with a single other retrieval wavelength range. Furthermore, a large variety of retrieval wavelength intervals have been used by different authors. This is illustrated by Table 1, which displays a selection of different retrieval wavelength ranges of bromine monoxide (BrO), which have been used in the past. Since the studies of BrO in Table 1 have been performed with different instruments from different platforms and strongly varying measurement conditions, a single retrieval wavelength interval would not have been sufficient. Nevertheless, one wonders whether a the total of 32 different retrieval wavelength intervals really represents the different requirements of the various measurement geometries and instruments used.

One of the few systematic studies for the retrieval of BrO was published by Aliwell et al. (2002), where DOAS retrievals were studied for measurements of stratospheric BrO via ground based zenith-looking instruments at mid-latitudes. In that case, one faces low BrO SCDs combined with very high ozone (O_3) SCDs which interfere with the evaluation since measurements are conducted at a high solar zenith angles (SZA). Aliwell et al. (2002) found an optimal retrieval range from 346 nm to 359 nm, which limits interferences with O_3 but encompasses only two, relatively weak BrO absorption bands in the retrieval. Theys et al. (2007) supported the suggested wavelength range with an additional radiative transfer study. The results of this study, however, can not be unambiguously transferred to the retrieval of BrO under different measurement conditions (e.g. differences in BrO SCDs, SZA, time difference between measurement of Fraunhofer reference spectrum and measurement spectrum, etc.). Similar studies for other measurement conditions and trace gases are sparse. Furthermore, the effects of

AMTD
5, 4195–4247, 2012

different retrieval intervals have not been studied systematically over a broad range of retrieval intervals for any trace gas.

In this study, we introduce a novel tool which is suitable to systematically and quantitatively study the influence of the retrieval wavelength interval on the results and quality of the DOAS retrieval. It consists of contour plots of DOAS retrieval results where the lower and upper limits of retrieval wavelength intervals are the coordinates, while the value of retrieved column density or the value of any other retrieval parameter of interest (e.g. fit error, χ^2 value, possible shifts in wavelength calibration by the algorithm) is plotted colour-coded (see Sect. 2). These retrieval-maps enable an easy visualization of results for a large set of evaluation wavelength ranges and thus offer an intuitive tool to show how certain key parameters influence the fit results.

One problem when analysing the influence of the retrieval wavelength range is that the true SCDs of trace gases are usually unknown for measured spectra. Therefore, as an application example, synthetic spectra are studied with known columns of trace gases. These synthetic spectra represent simplified spectra of passive DOAS measurements of stratospheric BrO and BrO in volcanic plumes using scattered sunlight (see Sect. 3). Different tests are performed on these synthetic spectra as described in Sect. 3.3. Namely, (i) the influence of the I_0-effect, (ii) cross correlations between trace gas RCSs and variations in assumed trace gas SCDs, and (iii) the behaviour of retrieved results when noise is added to the synthetic spectra. The results for each measurement set-up and test are presented and discussed in Sect. 4, followed by a general comparison between measurement scenarios in the subsequent Sect. 5 and concluding remarks (Sect. 6).

2 Retrieval wavelength mapping – general approach

Small errors in reference cross sections (RCSs) and corrections for broad band extinction, unaccounted radiative transfer effects, cross correlations between RCSs and instrumental defects may lead to erroneously retrieved slant column densities (SCDs)

AMTD
5, 4195–4247, 2012

of measured trace gases. In general, these systematic errors exhibit a dependency on the retrieval wavelength interval, which varies slower over broader wavelength intervals than errors introduced by common pixel to pixel electronic or photonic noise. Therefore, these different types of error should be distinguishable in a systematic study of the influence of retrieval wavelength intervals on the retrieved values.

A DOAS retrieval performed systematically over a wide range of different wavelength ranges may uncover these systematic variations and allows to study key parameters. E.g., this includes among others the retrieval wavelength interval dependency of

- retrieved trace gas SCDs and their fit error,
- cross correlations between different RCSs,
- the influence of parameters like wavelength calibration of spectra,
- radiative transfer effects,
- influence of instrumental features,
- shifts in wavelength calibration of recorded spectra by the retrieval algorithm,
- dependency of the retrieved values on the I_0-effect and Ring-effect (Passive DOAS measurements only).

By studying appropriate parameters, an optimal retrieval wavelength range may be found which results in a robust retrieval of true trace gas slant columns. Potential lies in an optimal homogenization of the retrievals, in case larger data sets are studied which were recorded by different instruments.

Easy visualization of such systematic retrievals can be achieved by displaying the results in contour plots, where the first and second dimension are the lower and upper limits of the retrieval wavelength interval, respectively. The results are plotted colour coded. Thus each point in the plot corresponds to one particular wavelength interval. The resulting maps allow to readily identify retrieval wavelength intervals which are

AMTD
5, 4195–4247, 2012

likely to lead to erroneous results, or might lead to greater variability of retrieved values due to a large gradient of the retrieval interval dependency.

As an example of this novel method, Fig. 1 displays retrieved BrO SCDs using a synthetic spectrum modelling zenith-sky DOAS measurements of stratospheric BrO. Details on the construction of the synthetic spectrum are given in Sect. 3. Since it is a synthetic spectrum, the true BrO SCD of 1.5×10^{14} molec cm^{-2} is known. All retrieval wavelength intervals are plotted with lower limits of 316–358 nm and upper limits of 322–364 nm. The respective wavelength limits are varied in steps of 0.1 nm, with a total width of the interval ω between 6 nm and 45 nm. Retrieval results which differ by less than 0.1 % from the true SCD are plotted in white; under- and overestimated results in shades of blue and red, respectively. The BrO absorption cross section is plotted at abscissae and ordinate of the graph for orientation. The advantage of this systematic approach is apparent: In a first assessment, certain retrieval wavelength intervals can be disregarded since they yield results quite strongly deviating from the true value, others could be subject to further investigation. For instance, evaluation intervals including wavelengths below ≈345 nm yield erroneous results. For an in depth discussion of the depicted result, see Sect. 4.1.

Computational requirements to map the wavelength evaluation ranges are moderate. All shown individual maps were generated on a desktop PC with a 3.0 GHz processing unit. The retrievals necessary for a single map were performed with the software package DOASIS (Kraus, 2006) within 30 min for given wavelength evaluation ranges at 0.1 nm steps. Therefore this novel tool allows to give a quick overview of possible pitfalls in DOAS evaluations.

3 Retrieval wavelength mapping at the example of synthetic spectra

In order to give an example application of the above described method, synthetic spectra were generated simulating two different measurement scenarios: Stratospheric BrO by zenith-sky DOAS and BrO in tropospheric volcanic plumes. As mentioned above,

AMTD
5, 4195–4247, 2012

synthetic spectra offer the advantage that retrieved and true SCDs can be compared. Both measurement scenarios assume passive DOAS measurements using scattered sunlight, allowing to study the two different measurement conditions in direct comparison. In order not to exceed the scope of these examples, certain effects are neglected. This is most importantly the Ring-Effect (Grainger and Ring, 1962), which, if insufficiently corrected, may greatly affect the retrieval results due to its narrow band structure. Furthermore, the effects of noise are neglected for certain tests (I and II, see Sect. 3.3) performed on the two measurement scenarios. Given these simplifications, the results can be assumed to yield the lowest error possible and act as a "best case" scenario. This poses certain limits on the application of studied synthetic measurement scenarios to measured spectra, but the prime focus in this study is to present the new method of retrieval wavelength mapping rather than model real measurement spectra.

The software package DOASIS was used for computation of all spectra and retrieval of results (Kraus, 2006; Lehmann, 2012).

3.1 Generation of synthetic spectra

The same approach was taken for all measurement scenarios in constructing synthetic spectra as well as RCS. Because this study focuses on measurements using scattered sun light, a high resolution solar spectrum $I_{K,0}$ (Kurucz, 2005) is used as an initial spectrum without additional absorption structures with $\approx 3 \times 10^5$ pixels between 300 and 450 nm. The literature absorption cross sections of the different trace gases ($\sigma_i(\lambda)$, see Table 2) were recorded at different spectral resolutions. Thus they were first interpolated to $\sigma_{K,i}(\lambda)$ at the resolution of the initial solar spectrum $I_{K,0}$. Subsequently, the RCSs $\sigma_{K,i}(\lambda)$ were multiplied with the respective SCDs S_i assumed for each trace gas and measurement scenario. Their absorptions were applied to the solar spectrum $I_{K,0}$ according to Lambert-Beer's Law:

$$I_K(\lambda) = I_{K,0}(\lambda) \exp\left(-\sum_i \sigma_{K,i}(\lambda) \cdot S_i\right) \quad (1)$$

AMTD
5, 4195–4247, 2012

The high resolution spectra with (I_K) and without absorptions ($I_{K,0}$) were convolved with an instrumental slit function W of Gaussian shape with 0.65 nm FWHM. A spectrometer with a detector of 1024 pixels was assumed with a spectral range of 300–402.3 nm with a constant dispersion of 0.1 nm pixel^{-1}. This allows to disregard possible undersampling effects (Roscoe et al., 1996; Platt et al., 1997; Chance et al., 2005). The thus calculated synthetic spectra are denoted I_0 and I_M for Fraunhofer reference and measurement, respectively.

When convolving the high resolution RCSs $\sigma_{K,i}(\lambda)$ to the resolution of the instrument, care must be taken to account for the I_0-effect (Platt et al., 1997), because the incident solar spectrum and the RCSs are highly structured. The convolution also introduces an error for absorbers at high optical densities ($\ln(I/I_0) > 0.1$). The reason for both effects is that the convolution and Lambert-Beers-law do not commute (e.g. Wenig et al., 2005). In this study, RCSs are denoted as "uncorrected RCSs" if they are not corrected for the I_0-effect or saturation effect. They are constructed by convolving the RCSs $\sigma_{K,i}(\lambda)$ with the instrumental slit function W to the instrumental resolution.

RCSs corrected for the I_0-effect and saturation are calculated corresponding to (Platt et al., 1997; Aliwell et al., 2002; Wagner et al., 2002):

$$\sigma'_i(\lambda) = -\frac{1}{S_i} \ln \left(\frac{([I_{K,0} \exp(-\sigma_i S_i)] * W)(\lambda)}{(I_{K,0} * W)(\lambda)} \right) \quad (2)$$

where $*$ denotes the convolution operation. However, using only the incident solar light $I_{K,0}$ in the denominator of Eq. (2) neglects the fact that many absorbers can be present at partly very high optical densities (e.g. O_3 in the measurement scenario for zenith-sky DOAS, Sect. 3.2.1). Thus a true correction of the I_0 effect, can only be achieved if a spectrum $I_{K',0}$ is used in Eq. (2), which consists of $I_{K,0}$ modified by all other absorptions present, except the one to be corrected. Although this can easily be achieved for synthetic spectra with known SCDs of absorbers, it would require a high computational effort applied to measured spectra, which is not feasible for common DOAS retrievals.

AMTD
5, 4195–4247, 2012

3.2 Measurement scenarios

3.2.1 Measurements of stratospheric BrO by zenith-sky DOAS

In this scenario, spectra of ground based zenith-sky DOAS measurements are simulated, which are used to measure stratospheric BrO. Commonly, spectra are recorded with a zenith looking telescope at high solar zenith angles (SZA). Evaluation of spectra at higher SZA against reference spectra at e.g. 70° SZA yield information about stratospheric trace gases. The main problem for retrievals of stratospheric BrO measurements are the encountered strong O_3 absorption structures at lower wavelengths. The results can be transferred to other measurement scenarios under similar conditions (e.g. stratospheric Balloon measurements, Satellite measurements in limb-viewing direction). Information on the assumed RCS and SCDs are given in Table 2. The assumed values for the zenith-sky DOAS scenario are the same as the ones used in a previous study by Aliwell et al. (2002). However, instead of the BrO cross section by Wahner et al. (1988) at 223 K, the cross section by Fleischmann et al. (2004) at 298 K was used, because the latter is available in higher resolution and the same BrO cross sections for both measurement scenarios can be used. Sensitivity tests have been performed for cross sections at different temperatures and by different authors (Wahner et al., 1988; Wilmouth et al., 1999; Fleischmann et al., 2004). Although the amplitude can differ significantly, the shape remains similar (see also Dorf, 2005). Since BrO optical density is small compared to the other absorbers, it can be assumed that the relative changes in retrieved SCDs are independent of the respective BrO RCSs used for all tests performed. This approach is justified by the negligible differences in retrieved SCDs that can be seen in the later presented results between this study and (Aliwell et al., 2002), Sect. 4.1.1.

AMTD
5, 4195–4247, 2012

3.2.2 BrO in tropospheric volcanic plumes

This scenario is set up to model tropospheric measurements of a volcanic plume at low elevation viewing angles. The reference Fraunhofer spectrum would be recorded in zenith view, and it is assumed that both spectra are taken in close proximity in time and thus at approximately the same SZA. Consequently, the measurement will be sensitive to trace gases in the volcanic plume as well as to absorbers in the the lower ambient atmosphere. Stratospheric absorptions should be the same in both, measurement and reference spectrum and cancel in the retrieval. Thus they are neglected in this scenario. Tropospheric SCDs of NO_2, O_3 and HCHO correspond to a slightly polluted troposphere, as e.g. found at Mt. Etna, Italy, during the summer months (Huijnen et al., 2010; Curci et al., 2010; Heckel et al., 2005). BrO and SO_2 SCDs are typical for a diluted plume, which is several minutes old at the point of the measurement (e.g. Bobrowski and Platt, 2007; von Glasow, 2010). Advanced modelled measurement scenarios are described in Vogel (2011).

These measurement conditions are quite different to those of zenith-sky DOAS. Since stratospheric O_3 absorptions are neglected, assumed SCDs of tropospheric O_3 are much smaller. However, the volcanic plume includes SO_2 at high concentrations, which absorbs in a similar wavelength range as O_3. Also possible cross correlation of BrO with ambient HCHO must be taken into account due to similar shape of absorption structures and encountered optical density.

3.3 Tests performed on synthetic spectra

Several tests were performed on the two measurement scenarios. In order to allow a better comparison between the different tests, only two different retrievals are used. Applied are a set of (1) uncorrected RCSs and (2) I_0 corrected RCSs for each scenario. The different tests vary by small changes to the synthetic measurement spectra (variations of the SCDs of absorbers, added noise, etc.). Otherwise, all retrievals are performed coherently. In both evaluation scenarios, the logarithm of the Fraunhofer

AMTD
5, 4195–4247, 2012

reference spectrum I_0 was fitted together with the RCSs to the logarithm of the synthetic measurement spectrum I_M instead of fitting the RCSs to the logarithm of the ratio I_M/I_0. This is a common approach in order to account for small shifts in wavelength pixel mapping between Fraunhofer reference and measurement spectrum, which can occur, e.g. by temperature drifts of the optical bench of the spectrograph. The fit coefficient of the Fraunhofer reference was fixed to unity. Stability of the retrieval was ensured by only allowing the set of RCS and Fraunhofer reference spectrum to shift and squeeze in wavelength as a whole. Furthermore, a DOAS polynomial of second order was included. This is sufficient since no additional broad band extinctions are applied during the construction of synthetic spectra.

3.3.1 Test I, influence of the I_0-effect

As a first test, the influence of the I_0-effect on retrieved column densities was assessed by fitting both sets of RCSs (uncorrected and corrected for the I_0-effect) to the synthetic measurement spectrum. In this way, the upper limit of accuracy is established at which the different SCDs of respective measurement scenarios can be reproduced. Also, this test allows direct comparison to the study of Aliwell et al. (2002) for the zenith-sky DOAS measurement set-up.

3.3.2 Test II, interferences of other absorbers on retrieved BrO SCD

Beyond the behaviour of retrieved trace gas SCDs with changing evaluation wavelength intervals, many other properties of a fit can be investigated (see above). Test II is designed to yield information on the sensitivity of the retrieval to small variations of the amount of absorbers present. Cross correlations between the differential absorption cross sections of the different absorbers may affect the retrieved SCDs. Since the RCSs are wavelength dependent, these cross correlations are depending on the retrieval wavelength range.

AMTD
5, 4195–4247, 2012

A series of fits were used to assess these cross correlations: the original sets of RCSs (uncorrected and I_0 corrected) were fitted to synthetic spectra, which were constructed with varying strengths of absorbers. Dependencies of retrieved BrO SCDS on other absorber strengths can be expressed as

$$\frac{\delta S_{\mathrm{BrO}}}{\delta S_A} = \frac{S_{\mathrm{BrO},A+} - S_{\mathrm{BrO},A-}}{2\Delta S_A} \cdot \left(\frac{S_{\mathrm{BrO},0}}{S_{A,0}}\right)^{-1} \tag{3}$$

The derivative δS_{BrO} to variations in columns of absorber A (δS_A) is calculated from BrO SCDs $S_{\mathrm{BrO},A+}$ and $S_{\mathrm{BrO},A-}$, which are retrieved when changing the original SCDs of absorber A $S_{A,0}$ by $\pm\Delta S_A$, respectively. $S_{A,0}$ and $S_{\mathrm{BrO},0}$ are the SCDs as given in Table 2. The sensitivity of the BrO SCD at a certain retrieval wavelength range to changes in SCDs of all other absorbers is estimated by

$$\frac{\mathrm{d}S_{\mathrm{BrO}}}{\mathrm{d}S_{\mathrm{All}}} = \frac{1}{n_A} \sum_{\mathrm{A}} \frac{\delta S_{\mathrm{BrO}}}{\delta S_A} \tag{4}$$

where n_A denotes the total number of different absorbers excluding BrO.

An additional error is introduced by varying the absorbers while constructing the synthetic measurement spectrum without changing the I_0 correction of RCSs in the respective fit scenario. Thus the dependencies revealed are resulting from (1) cross correlations between different RCSs and (2) wrongly assumed trace gas SCDs when correcting for the I_0-effect of the respective trace gas.

The variations of the trace gases were set to 1 % for the measurement scenarios assessing stratospheric BrO by zenith-sky DOAS and 10 % for the measurement scenarios of BrO in volcanic plumes (see also Table 2). For real measurement spectra, additional residual structures and noise may increase these cross correlations. Thus this test will only yield a "best case" result.

AMTD
5, 4195–4247, 2012

3.3.3 Test III, effect of noise on retrieval and error calculation

In order to render the theoretical study more realistic, tests were performed on the synthetic spectra with added noise. Typical residual structures are simulated by adding Gaussian noise to the logarithm of the measurement spectra. The standard deviation of the noise structure was normalized to 3×10^{-4} optical density. Additional broad band features were introduced by binomial low pass filtering (e.g. Jähne, 2005) of the noise with 0, 10 and 50 iterations with subsequent rescaling (see Fig. 2). 10 and 50 iterations correspond to a filtering using a running mean of 6 and 15 pixels, similar to the error calculation study by Stutz and Platt (1996). For an average FWHM of 1.5 nm (15 pixels) of one BrO absorption band, the correction factor given by Stutz and Platt (1996) is ≈1.5 for unfiltered noise, ≈2.5–3 for noise filtered with 10 iterations and ≈4.5 for 50 iterations, respectively.

The influence of noise on retrievals with I_0 corrected and uncorrected RCSs was tested only for the case of unfiltered noise. Broader residual structures are studied only for I_0 corrected RCS. In order to get reasonable statistics with independent retrieval results for each wavelength retrieval range, 100 maps with independent noise for each wavelength range are averaged on the retrieval map.

4 Results and discussion of the individual measurement scenarios

Results of the different tests are presented in the following section, which were performed on the measurement scenarios zenith-sky DOAS (see Sect. 4.1) and DOAS measurements of volcanic plumes (see Sect. 4.2).

AMTD
5, 4195–4247, 2012

4.1 Zenith-sky DOAS

4.1.1 Test I, influence of the I_0-effect on zenith-sky DOAS

Figures 1 and 3 depict the deviation from the true BrO SCD of 1.5×10^{14} molec cm^{-2} for I_0 corrected and uncorrected RCSs used in the retrieval, respectively. In case of I_0 corrected RCSs (see Fig. 1), retrieved BrO SCDs vary by more than 10 % at most retrieval ranges including wavelengths below 330 nm. If fits are only performed at longer wavelengths, deviations of less than 1 % are achieved for lower limits >345 nm. Note that no additional residual structures or noise has been added in this test and therefore the results can be regarded as an lower limit of accuracy. The observed deviations can be attributed mainly due to an slightly erroneos correction of the I_0-effect since the denominator in the correction (Eq. 2) consists only of the incident solar light without the presence of other absorbers.

If uncorrected RCSs are applied in the fitting algorithm (Fig. 3), the retrieval of the true BrO SCD is not unambiguously possible. Highly erroneous results by more than 100 % are to be expected for retrieval wavelength intervals including wavelengths below ≈340 nm. Even at longer wavelengths, most wavelength intervals yield values deviating by more than 20 % from the true BrO SCD.

For both sets of RCSs, one of the major features visible in the retrieval maps is that the results are depending mostly on the lower wavelength limit. This is again an indication for the influence of the strong O_3 absorptions, because their absorption structures are decreasing with increasing wavelength. Preferences to under- or overestimate the true BrO SCD are changing with the in the retrieval wavelength interval included BrO absorption maxima.

Figure 4 depicts retrieval results and residuals at the example of three different wavelength ranges for both, uncorrected and I_0 corrected RCSs. The evaluation wavelength intervals chosen correspond to the ones marked by #11 (319–347.5 nm), #5 (332–352 nm) and #9 (346–359 nm) in Table 1, Figs. 1 and 3. Greater residual structures occurring for the retrieval between 319 nm and 347.5 nm confirm that retrievals at lower

AMTD
5, 4195–4247, 2012

wavelength ranges and use of uncorrected RCSs must be avoided if higher O_3 absorptions are present in the measurement spectra, even in this "best case" using synthetic spectra without noise. The residuals of the retrievals using other wavelength intervals than 346–359 nm still show strong residual structures if I_0 corrected RCSs are applied in the fitting process. The residual structures of the retrieval using uncorrected RCSs at 346–359 nm reproduce the results of test C1 and C2 described in (Aliwell et al., 2002), both in retrieved BrO SCD and shape of residual.

The previous study by Aliwell et al. (2002) recommended the use of a retrieval wavelength interval between 346 nm and 359 nm (#9 in Figs. 1 and 3) due to greater stability of retrieved SCDs in measured spectra. This evaluation wavelength range is well studied and validated (e.g. Theys et al., 2007). However, if strong O_3 absorptions are present, care must be taken to apply a valid I_0 correction to the RCSs. Otherwise the retrieval may overestimate the true BrO SCD.

4.1.2 Test II, interferences of other absorbers for zenith-sky DOAS

In this test, the dependencies of the retrieved column density of the trace gas of interest (i.e. BrO) on changes in other absorber strengths were investigated. Figure 5 depicts the relative change in retrieved BrO SCD when varying the strength of the other absorbers in the synthetic measurement spectrum by 1 %. Note that only I_0 corrected RCSs are used in the fitting algorithm. If any of the O_3 RCSs are varied by 1 %, a relative change of BrO of more than 10 % occurs for wavelength ranges of a lower limit between 316–330 nm. Even above a lower wavelength interval limit of 330 nm changes of BrO SCDs greater than 10 % are present for O_3 at 221 K, the stronger of the two O_3 RCSs used. Relative changes of BrO SCD due to O_3 at 241 K remain mostly below 5 % above a lower limit of ≈335 nm and become negligible above 345 nm. Therefore the variations of SCDs for the zenith-sky DOAS scenario show a clear imprint of the strong O_3 absorptions. They generally lead to an overestimation of BrO SCDs if wavelengths <330 nm are included in the retrieval. The strong O_3 absorptions also affect the retrieved BrO SCDs at longer wavelengths, although not as severly. The shown

AMTD
5, 4195–4247, 2012

differences are resulting from a combination of slightly erroneous I_0 correction (the original SCDs are used, $I_{K,0}$ in Eq. (2) neglects presence of other absorbers) and possible cross correlation of absorption cross section, which are not resolved in this test.

Compared to O_3, the influence of varying NO_2 SCD is only minor and can be disregarded when evaluating at intervals starting above a lower limit of 345 nm. However, the depicted dependency of NO_2 at the shorter wavelength end of the evaluation range is surprising. Other than O_3, the differential optical absorption bands of NO_2 increase in strength towards longer wavelengths. Thus a dependency on the upper wavelength end of the evaluation retrieval would be expected. The observed deviations from the true SCDs are most likely resulting from an insufficient correction of the I_0-effect of the strong O_3 absorptions. Indications are the structures observed already in the plots for varying O_3 strengths.

4.1.3 Test III, effect of noise on retrieval and error calculation for zenith-sky DOAS

Figure 6 depicts the retrieved BrO SCDs if additional noise structures are added to the synthetic spectra. In order to obtain significant results, retrievals were performed at each individual wavelength interval with 100 different noise spectra. The first column shows the results if uncorrected RCSs are applied together with unfiltered noise, whereas the following columns depict fits applying I_0 corrected RCS with unfiltered Gaussian noise, followed by low pass filtered Gaussian noise with a binomial filter of 10 and 50 iterations, respectively (for noise examples, see Fig. 2). The top row gives the mean of resulting BrO SCDs, the middle row shows the standard deviation for the respective wavelength retrieval interval and the bottom row gives the correction factor defined by Stutz and Platt (1996), which is the ratio of standard deviation of results and the mean fit error.

Comparing the retrieved BrO SCDs from synthetic spectra without noise (Test I) and with the different structured noise types, the mean BrO SCDs of the noisy spectra do not differ from the ones without noise, regardless whether RCS are corrected or not

AMTD
5, 4195–4247, 2012

for the I_0 effect (Figs. 1 and 3). The noise only leads to an increased scatter of results, which can clearly be observed for the I_0 corrected RCS, column 2 till 4. This agrees with the intuitive expectation that the average should remain the same, because although the individual noise spectra exhibit wavelength depending structures, they do not share systematic, wavelength depending features. An increase in standard deviation of results is observed, but also the variations observed in Figs. 1 and 3 are more apparent with increasingly structured noise. Whereas the average BrO SCDs around a lower retrieval wavelength limit of 332.5 nm for all upper limits (thus following a vertical line) do not deviate from the results of synthetic spectra without noise, the average of the retrieval starts to systematically underestimate the results with increasing noise structure. The same is true for an overestimation of values between lower limits of 334–338 nm. This indicates that underlying systematic errors are not concealed by noise but actually become more pronounced. The reason for this is yet unclear.

The standard deviation shows a clear change at ≈338 nm, 345 nm and 350 nm of lower limit of the retrieval interval for all cases studied (different noise types, uncorrected and I_0 corrected RCS). These changes correspond to the maxima of different BrO absorption bands included in the fitting process. Comparing standard deviations of uncorrected and I_0 corrected RCS, no major difference can be observed. Therefore, the unstructured noise does not obviously influence the distribution of retrieved values even if systematic structures are present. Nevertheless, the systematic structures influence the fit error greatly. This can be observed in Fig. 6 by looking at the correction factor, the ratio between standard deviation and fit error (see Sect. 3.3). For unfiltered noise, a correction factor below 1 is calculated for evaluations of lower limit <330 nm for I_0 corrected RCS, and even a factor below 1 for all evaluations of lower limit <345 nm for uncorrected RCS. A possible reason for this behaviour is discussed in Sect. 5.

AMTD
5, 4195–4247, 2012

4.2 BrO in volcanic plumes

4.2.1 Test I, influence of the I_0-effect on retrievals of BrO in volcanic plumes

Figure 7 shows the results for the measurement scenario of BrO in volcanic plumes for a retrieval using I_0 corrected RCSs. It is apparent that the I_0 corrected retrieval yields results with only minor deviations from the true BrO SCD at most evaluation wavelength intervals. The deviations range up to 1 % only if the fit is performed with a retrieval interval starting below ≈323 nm. These features may be attributed to the stronger SO_2 and O_3 absorptions at shorter wavelengths. Compared to the zenith-sky DOAS scenario applying I_0 corrected RCSs (Fig. 1), the combined SO_2 and O_3 differential absorptions are still an order of magnitude smaller than the combined O_3 differential absorptions in the zenith-sky DOAS scenario, which reduces the deviations of BrO SCDs due to an insufficient I_0 correction. Also residual structures shown for three different evaluation wavelength ranges are negligible (Fig. 9).

If uncorrected RCSs are used, the retrieved BrO SCDs show larger deviations from the true BrO SCD (Fig. 8), however far less than observed in the scenario for zenith-sky DOAS (Fig. 3). In general, a systemic overestimation of BrO SCDs is apparent if wavelengths below 319 nm and above 332.5 nm are included in the retrieval, whereas otherwise BrO SCDs are slightly underestimated. Deviations from the true BrO SCD range of more than 10 % are only observed at lower limits >347.5 nm and in the range of lower limits >332.5 nm and upper limits <345 nm. Assigning deviations at a specific retrieval wavelength range to a certain trace gas is difficult since possible cross correlations may occur between all trace gases. Also, changes in retrieved SCDs of absorbers do not directly translate to the same changes in the respective optical density of the differential optical absorption structure due to the wavelength dependency of the RCSs. As an example, optical densities are given in Table 3 for different trace gases at three different wavelengths. An attempt to assign different wavelength intervals to different absorbers most interfering with the BrO retrieval at respective wavelength ranges is

AMTD
5, 4195–4247, 2012

presented in Appendix A. It shows, e.g. that the observed deviations from the true BrO SCD in Fig. 8 may be caused by cross correlations between RCSs of BrO and HCHO.

Figure 9 displays fit examples for uncorrected and I_0 corrected RCSs. As expected from the previously shown Figs. 7 and 8, only small residual structures and deviations from the true BrO SCD are observed. For the retrievals applying I_0 corrected RCSs, all three different retrieval wavelength ranges yield negligible residual structures. In contrast to the fit examples of the zenith-sky DOAS scenario (Fig. 4), the retrieval wavelength interval between 332 nm and 352 nm is most accurate and the wavelength interval of 346–359 nm shows the largest deviation from the true BrO SCD. The differences may be explained by the presence of the additional absorber HCHO in the studied scenario, the RCS of which shows an anti-correlation to the BrO RCS.

4.2.2 Test II, interferences of other absorbers when evaluating BrO in volcanic plumes

As described in the previous paragraph, I_0 corrected RCSs yield accurate results with only slight deviation from the true BrO SCD when lower wavelengths are included (<325 nm, Fig. 7). These results are also confirmed when varying the strengths of other absorbers in the case of the scenario for volcanic plumes. The influence of changes in other absorber strength on the retrieved BrO columns is visible for I_0 corrected RCSs in Fig. 11. The increased absorptions of O_3 and SO_2 below 325 nm lead to a small overestimation of BrO SCDs if these wavelengths are included in the retrieval wavelength interval. In the case of NO_2, almost all wavelength intervals show an anti-correlation with BrO. The absorption structure of NO_2 is rather complex and does not show clearly overlapping absorption bands with BrO. Nevertheless, NO_2 interacts unfavourably with BrO due to its comparably high optical density (Table 3). BrO shows the least dependency on changes in absorber strength to HCHO. Interferences are mainly observed at shorter wavelength limits between 335–340 nm and above 345 nm. This may be attributed to absorption bands of similar shape for both trace gases at ≈338 nm. However, these results stand in contrast to findings using measured spectra, where much higher

AMTD
5, 4195–4247, 2012

anti-correlations can be expected (Vogel, 2011). It can be speculated, that cross correlations between HCHO and BrO are observed when systematic residual structures are present (see also Sect. 5 and Appendix A).

The average of all dependencies in Fig. 10 is shown in Fig. 11. BrO SCDs obtained in retrieval wavelength intervals with a lower limit <325 nm are dominated by O_3 and SO_2 features, where as results at other wavelength intervals may be influenced mainly by NO_2 and HCHO. An area least affected by varying absorber strengths is observed between lower limits of 326 nm and 333 nm. However, interferences in total remain negligible as long as the stronger differential absorption structures of SO_2 and O_3 are avoided.

4.2.3 Test III, the effect of noise on retrieval and error calculation for BrO in volcanic plumes

The effect of different noise spectra on the retrieval of BrO in volcanic plumes are depicted in Fig. 12. As already observed for the scenario of zenith-sky DOAS, Sect. 4.1.3, certain weak variations of BrO SCDs are becoming more pronounced by the induced noise, as can be seen comparing Fig. 8 with Fig. 12 for the case of an evaluation using uncorrected RCSs. Possible minor deviations from the true BrO SCDs for evaluations applying I_0 corrected RCSs are still concealed by the noise.

Comparing the standard deviations for retrievals using uncorrected and I_0 corrected RCSs (Fig. 12e, f), no differences can be distinguished, although results for both types of evaluations differ (Fig. 12a, b). Therefore the unfiltered noise leads to comparable standard deviation of retrieved BrO SCDs but absolute results are dominated by the underlying systematic residuals. In the case of the I_0 corrected RCSs, the average values remain the same, independent of the different filtered noise spectra. A general increase in standard deviation is visible with an increase in structure of the noise spectra (i.e. stronger low pass filtering). For all types of noise spectra, a sudden increase in standard deviation occurs at a shorter retrieval wavelength limit of 338 nm and 345 nm,

AMTD
5, 4195–4247, 2012

corresponding to a decrease in amplitude of the differential optical absorption bands of BrO included in the fit.

The calculated correction factor shows a clear transition at a lower limit of 320 nm for uncorrected RCSs, changing from below unity to an average value of 1 for all other retrieval wavelength intervals. For wavelength intervals incorporating wavelengths <320 nm, strong SO_2 and O_3 induce residual structures, which increase the fit error. Since the standard deviation is not affected, the correction factor to give the true measurement error is lower than expected by a previous assessments by Stutz and Platt (1996).

For I_0 corrected RCSs, the correction factor only shows a small wavelength dependence. For unfiltered noise, standard deviation and measurement error do not differ significantly, for low pass filtered noise (10 and 50 iterations of the binomial filter), correction factors of ≈3 and ≈4.5 need to be applied to calculate the true standard deviation from the fit error. This agrees well with the error estimations by Stutz and Platt (1996) since here the systematic structures due to an insufficient I_0 correction of RCSs are negligible.

5 Comparison of results from both measurement scenarios

The three tests for both measurement scenarios yield several common features. Even if generalisations are difficult without a thorough mathematical description, these findings offer empirical insights and reveal common pitfalls in DOAS evaluations.

5.1 I_0 corrected and uncorrected reference cross sections

Although the two measurement scenarios incorporate absorptions of differing strengths, retrieved SCDs showed that an I_0 correction should always be applied. This is especially true if very strong absorbers conceal the trace gas of interest (e.g. O_3 concealing BrO in the scenario zenith-sky DOAS). Even in this best-case study, an

AMTD
5, 4195–4247, 2012

insufficient correction of the I_0-effect yielded deviations of the BrO SCDs at lower wavelengths with high O_3 absorptions. In the case of the scenario of BrO in volcanic plumes, optical densities of the different absorbers are not exceeding the optical density of BrO by orders of magnitude at wavelenghts ≥320 nm. Therefore deviations of the retrieved BrO SCDs are much smaller than for the zenith-sky DOAS scenario. Nevertheless, I_0 correction of the RCSs remains mandatory to achieve correct results. Sensitivity tests were performed with true I_0 corrected RCSs as outlined in Sect. (3.1). Using these sets of RCSs, true SCDs of all trace gases could be retrieved at all wavelength intervals for both measurement scenarios.

5.2 Sensitivity to interfering absorbers

In both measurement scenarios, variations in the strengths of other absorbers affected the BrO retrieval. These errors in the retrieved BrO SCDs are due to a combination of cross correlations between the different absorbers and an I_0 correction of RCSs with slightly erroneous SCDs. The observed dependencies are up to two magnitudes greater for the zenith-sky DOAS scenario than for the measurement scenario of volcanic plumes. Since the contributions of cross correlations and I_0 correction have not been separated, it is not possible to assign observed dependencies clearly. However, the observed correlations are in general quite small. Since (1) the synthetic spectra in this test are constructed without noise or other wavelength depending residual structures and (2) the retrieval wavelength ranges studied are sufficiently large at >60 channels of the simulated detector, a precise retrieval of all absorbers should be possible. The only source of error remaining is the one induced by the insufficient I_0-correction of RCS (see also Appendix A). Thus for the case of measured spectra, it can be speculated that retrieval wavelength interval depending correlations between trace gases originate from systematic residual structures. Their source can be, e.g. changes of absorption strength with wavelength due to wavelength depending radiative transfer or insufficient correction for the Ring-Effect in case of passive measurements. An example are cross correlations between BrO and HCHO observed in measurements of volcanic

AMTD
5, 4195–4247, 2012

plumes (Vogel, 2011), which occur despite the negligible correlations observed in this theoretical study.

5.3 Influence of noise on the retrieval

In Sects. 4.1.3 and 4.2.3 the influence of noise on the DOAS retrieval was tested. For both scenarios, SCDs obtained from synthetic spectra without additional noise were comparable to the mean of retrieved values of a significant number of spectra with noise. These findings remained true also when noise spectra were calculated with additional, random broad band structures.

The relationship between standard deviation of retrieved SCDs, fit error and the correction factor used to calculate one from the other has been described in Stutz and Platt (1996). They found, that the true standard deviation of retrieved SCDs is always larger than the fit error. However, the authors assumed that no systematic residual structures are present. The results presented in Sects. 4.1.3 and 4.2.3 reveal several interesting features. (1) Comparing results from retrievals applying uncorrected and I_0 corrected RCSs, it can be seen that the standard deviation of the retrieved SCDs does not appear to be depend on systematic wavelength structures by the I_0 effect. (2) However, the increase of the fit error by these systematic structures may lead to a correction factor <1. Therefore, the application of a correction factor may lead to overestimation of the true standard deviation.

One has to keep in mind that the observed effects are not pronounced when systematic residual structures are small and thus the boundary conditions of the previous study are fulfilled. In that case, the correction factor calculated for the BrO retrieval corresponds to the previously published approach. It is only dependent on the width of the differential absorption structure and width of the residual features, here ≈1.5 for unfiltered noise, ≈2.5–3 for noise filtered with 10 iterations and ≈4.5 for 50 iterations.

To perform an extensive error analysis on a theoretical basis is beyond the scope of this work. However, based on the empirical studies performed here, we conclude that correction factors calculated assuming only random structures should also be applied

AMTD
5, 4195–4247, 2012

if systematic residual structures are present. This approach may lead to an overestimation of the standard deviation of results, but the systematic spectral structures will also lead to a systematic offset of the average retrieved columns.

5.4 Recommended retrieval wavelength intervals

For zenith-sky DOAS, the tests confirmed the evaluation wavelength range 346–359 nm as suggested by Aliwell et al. (2002). This retrieval wavelength interval of BrO offers least dependency on the I_0 effect although an I_0 correction of RCSs is still mandatory. BrO retrievals including lower wavelengths are not advised since strong O_3 absorption and slightly insufficient I_0 correction of RCSs may yield highly erroneous values even in this "best-case" scenario.

BrO retrievals for measurement of volcanic plumes show a much lower I_0 dependency of the BrO SCDs on the retrieval wavelength interval, mostly due to an about 100-times weaker total O_3 SCD. Whereas the fit applying I_0 corrected RCSs shows a good agreement with the true BrO SCD at most wavelengths, misleading SCDs are retrieved for uncorrected RCSs. An evaluation wavelength interval with a lower wavelength limit between 320–335 nm is found to be optimal because here the differences are smallest between retrievals applying uncorrected and I_0 corrected RCSs. In practice, the absorber strength at short wavelengths is most variable because of the great variability of volcanic SO_2 emissions and O_3 absorptions in early and late hours of the day. To ensure a comparable evaluation of data, measurements should be performed at the upper range of suggested interval. However, a specific retrieval wavelength interval can not be recommended for the evaluation of BrO in volcanic plumes here. Advanced modelling of synthetic spectra (including realistic simulations of the atmospheric radiative transfer and the Ring effect) in comparison with measured spectra are needed in order to advice for a specific retrieval wavelength interval.

AMTD
5, 4195–4247, 2012

6 Conclusions

The retrieval wavelength interval is one of the most important parameters in a DOAS retrieval. Finding the optimal retrieval wavelength interval is not trivial, because many wavelength dependent effects may influence the retrieval, e.g. instrumental features, cross correlations between absorption cross sections and wavelength dependent radiative transfer. Previous publications motivated the applied wavelength retrieval interval by comparison with typically one or two additional wavelength intervals. The lack of appropriate visualisation prohibited a systematic study of the parameter space and made an easy determination of the optical retrieval wavelength interval extremely difficult.

In this study a novel method is presented, which consists of systematically varying the retrieval wavelength interval of DOAS retrievals and displaying the results in a contour plot. In this way, appropriate spectral intervals become immediately visible. Furthermore, the method is not limited to finding evaluation wavelength intervals by best values of resulting SCDs. Other parameters influencing the DOAS retrieval can be studied in the same way, e.g. interferences of absorption cross sections, effect of errors in I_0 correction, residual amplitude and shifts in wavelength-pixel calibration of the instrument.

In order to prove the concept, several tests were performed for two synthetic measurement scenarios of BrO by passive DOAS instruments. The scenario for zenith-sky DOAS reproduces conditions of stratospheric BrO measurements at mid-latitudes, where as the scenario of BrO in volcanic plumes captures typical conditions encountered when measuring BrO in tropospheric volcanic plumes. For the latter measurement scenario, this work constitutes the first systematic study of the dependency of retrieved BrO SCD on the retrieval wavelength interval. Tests on synthetic spectra included the assessment of the I_0 effect and the influence of its correction on the BrO retrieval. Furthermore, interferences between different absorption cross sections were

AMTD
5, 4195–4247, 2012

investigated and a statistical study was conducted on the influence of noise on the retrieval.

By studying synthetic spectra, interpretation of results is aided by knowledge of the SCDs applied to construct the spectra. Measured spectra usually lack this a priori knowledge and thus other approaches have to be chosen to obtain an optimal retrieval wavelength interval. E.g., for certain measurement conditions some trace gases should not be present. In the case of MAX-DOAS measurements, different Fraunhofer-reference-spectra can be compared, which should yield negligible differential SCDs, whereas night-time measurements of LP-DOAS systems should not yield BrO or other photochemically produced species.

At the example of synthetic spectra of passive DOAS measurements, the novel tool of retrieval wavelength mapping was introduced. However, the method is not limited to these types of instruments but can be applied to any DOAS measurement. Thus it enables a systematic study of important retrieval parameters, can highlight pitfalls in any DOAS retrieval and allows for an encompassing motivation of applied parameters.

Appendix A

BrO in volcanic plumes, Test I: Individual SCDs of all trace gases applying uncorrected RCSs

In Sect. 4.2.1 results are discussed of the retrieval using I_0 corrected and uncorrected RCSs. Here, an attempt is made to assign the observed deviations of retrieved BrO SCDs to individual trace gas absorptions present in the synthetic spectrum. Since the deviations for the retrieval using I_0 corrected RCSs are negligible, the discussion is restricted the retrieval applying uncorrected RCSs.

Table 3 shows the differential optical densities of all trace gases in the synthetic spectrum for three different wavelength intervals. These values serve as indications for the influence of the respective trace gas at these wavelengths. The individual retrieval

AMTD
5, 4195–4247, 2012

results for trace gases other than BrO are depicted in Fig. 13. Deviations from the true value (±1 %, denoted by the white color code) will influence the retrieval as a whole. In combination with the respective optical density, it indicates the influence of the respective trace gas to erroneous retrieval results in general.

SO_2 and O_3 absorptions influence the retrieval of BrO if shorter wavelengths (<325 nm) are included in the retrieval wavelength interval, although by far not as strong as in the case of the scenario zenith-sky DOAS. Due to the overall decrease in absorption cross sections with longer wavelengths for both species, their influence is reduced at longer wavelengths. However, the optical density of O_3 is still comparable to the one of BrO at 338 nm. Strongly deviating SCDs are retrieved for SO_2 above 335 nm (Fig. 13), but its optical density at these wavelengths is negligible compared to other absorbers. If the retrieval includes longer wavelengths ($>\approx 355$ nm), it can be assumed that errors due NO_2 are becoming more pronounced since its differential optical density is increasing as well as an overestimation of SCDs occurs (see Fig. 13).

The absorption bands of HCHO have a shape very similar to BrO, which may lead to an anti-correlation of both trace gases. On the one hand, the overestimation of HCHO SCDs for evaluation intervals starting at a lower limit (approximately 320–335 nm) thus might decrease retrieved BrO SCDs in that area. On the other hand, underestimation of HCHO SCDs at lower limits >335 nm can increase BrO SCDs. These findings are reflected in Fig. 7, where BrO SCDs are generally below the true value in evaluation regions of a lower limit range between 320 nm to 335 nm and above for lower limits greater than 335 nm. Especially, overestimations of HCHO SCDs at a lower wavelength limit 327.5–332 nm and upper limit <350 nm correspond to underestimated BrO SCDs (Fig. 8). These results indicate that BrO-HCHO cross correlations may cause erroneous retrieval results at similar measurement conditions. However, since the deviations of BrO SCDs are a result of a combination of all trace gas cross correlations, it is not unambiguously possible to assign deviations in the retrieved BrO SCDs to an individual trace gas alone.

AMTD
5, 4195–4247, 2012

Acknowledgements. L. Vogel and H. Sihler contributed equally to this work. The authors would like to thank both the atmospheric chemistry group in Heidelberg and the satellite remote sensing group in Mainz for thorough discussions during the development phase of the presented method. Funding for this work is gratefully acknowledged, and has been provided in part by the SOPRAN project (#03F0611F, by the BMBF, the German Federal Ministry of Education and Research), the Network for Observation of Volcanic and Atmospheric Change (NOVAC) by the European Commission Framework 6 Research Program and the International Max Planck Research School for Atmospheric Chemistry and Physics, Mainz (Germany).

References

Afe, O., Richter, A., Sierk, B., Wittrock, F., and Burrows, J.: BrO emission from volcanoes: a survey using GOME and SCIAMACHY measurements, Geophys. Res. Lett., 31, L24113, doi:10.1029/2004GL020994, 2004. 4231

Aliwell, S., Roozendael, M. V., Johnston, P., Richter, A., Wagner, T., and Arlander, D.: Analysis for BrO in zenith-sky spectra: an intercomparison exercise for analysis improvement, J. Geophys. Res., 107, 4199, doi:10.1029/2001JD000329, 2002. 4199, 4204, 4205, 4207, 4211, 4220, 4231, 4233, 4235, 4238

Bani, P., Oppenheimer, C., Tsanev, V. I., Carn, S. A., Cronin, S. J., Crimp, R., Calkins, J. A., Charley, D., Lardy, M., and Roberts, T. R.: Surge in sulphur and halogen degassing from Ambrym volcano, Vanuatu, B. Volcanol., 71, 1159–1168, doi:10.1007/s00445-009-0293-7, 2009. 4231

Begoin, M., Richter, A., Weber, M., Kaleschke, L., Tian-Kunze, X., Stohl, A., Theys, N., and Burrows, J. P.: Satellite observations of long range transport of a large BrO plume in the Arctic, Atmos. Chem. Phys., 10, 6515–6526, doi:10.5194/acp-10-6515-2010, 2010. 4231

Bobrowski, N. and Platt, U.: SO_2/BrO ratios studied in five volcanic plumes, J. Volcanol. Geoth. Res., 166, 147–160, doi:10.1016/j.jvolgeores.2007.07.003, 2007. 4206, 4231

Boichu, M., Oppenheimer, C., Roberts, T. J., Tsanev, V., and Kyle, P. R.: On bromine, nitrogen oxides and ozone depletion in the tropospheric plume of Erebus volcano (Antarctica), Atmos. Environ., 45, 3856–3866, doi:10.1016/j.atmosenv.2011.03.027, 2011. 4231

Burrows, J., Richter, A., Dehn, A., Deters, B., Himmelmann, S., and Orphal, J.: Atmospheric remote-sensing reference data from GOME – 2. Temperature-dependent absorp-

AMTD

5, 4195–4247, 2012

tion cross sections of O-3 in the 231–794 nm range, J. Quant. Spectrosc. Ra., 61, 509–517, doi:10.1016/S0022-4073(98)00037-5, 1999. 4233
Chance, K.: Analysis of BrO measurements from the Global Ozone Monitoring Experiment, Geophys. Res. Lett., 25, 3335–3338, doi:10.1029/98GL52359, 1998. 4231
Chance, K.: OMI Algorithm Theoretical Basis Document – Volume IV, Tech. rep., Smithsonian Astrophysical Observatory, Cambridge, MA, USA, 2002. 4231
Chance, K., Kurosu, T., and Sioris, C.: Undersampling correction for array detector-based satellite spectrometers, Appl. Optics, 44, 1296–1304, doi:10.1364/AO.44.001296, 2005. 4204
Curci, G., Palmer, P. I., Kurosu, T. P., Chance, K., and Visconti, G.: Estimating European volatile organic compound emissions using satellite observations of formaldehyde from the Ozone Monitoring Instrument, Atmos. Chem. Phys., 10, 11501–11517, doi:10.5194/acp-10-11501-2010, 2010. 4206
De Smedt, I., Van Roozendael, M., and Jacobs, T.: Optimization of DOAS settings for BrO fitting from SCIAMACHY nadir spectra – Comparison with GOME BrO retrievals, Tech. rep., Belg. Inst. for Space Aeron., Brussels, Belgium, available at: http://www.oma.be/BIRA-IASB/Molecules/BrO/BIRA_SCIABrO.pdf (last access: June 2011), 2004. 4231
Dorf, M.: Investigation of Inorganic Stratospheric Bromine using Balloon-Borne DOAS Measurements and Model Simulations, Ph.D. thesis, Combined Faculties for the Natural Sciences and for Mathematics, Ruperto Carola University of Heidelberg, Germany, 2005. 4205
Fleischmann, O., Hartmann, M., Burrows, J., and Orphal, J.: New ultraviolet absorption cross-sections of BrO at atmospheric temperatures measured by time-windowing Fourier transform spectroscopy, J. Photochem. Photobiol. A, 168, 117–132, doi:10.1016/j.jphotochem.2004.03.026, 2004. 4205, 4233
Grainger, J. F. and Ring, J.: Anomalous Fraunhofer line profiles, Nature, 193, 762–762 doi:10.1038/193762a0, 1962. 4203
Hebestreit, K., Stutz, J., Rosen, D., Matveiv, V., Peleg, M., Luria, M., and Platt, U.: DOAS measurements of tropospheric bromine oxide in mid-latitudes, Science, 283, 55–57, doi:10.1126/science.283.5398.55, 1999. 4232
Heckel, A., Richter, A., Tarsu, T., Wittrock, F., Hak, C., Pundt, I., Junkermann, W., and Burrows, J. P.: MAX-DOAS measurements of formaldehyde in the Po-Valley, Atmos. Chem. Phys., 5, 909–918, doi:10.5194/acp-5-909-2005, 2005. 4206

AMTD
5, 4195–4247, 2012

Hegels, E., Crutzen, P., Klupfel, T., Perner, D., and Burrows, J.: Global distribution of atmospheric bromine-monoxide from GOME on earth observing satellite ERS-2, Geophys. Res. Lett., 25, 3127–3130, doi:10.1029/98GL02417, 1998. 4231

Hermans, C., Vandaele, A., and Fally, S.: Fourier transform measurements of SO_2 absorption cross sections: I. Temperature dependence in the 24 000–29 000 cm^{-1} (345–420 nm) region, J. Quant. Spectrosc. Ra., 110, 756–765, doi:10.1016/j.jqsrt.2009.01.031, 2009. 4233

Heue, K.-P., Brenninkmeijer, C. A. M., Baker, A. K., Rauthe-Schöch, A., Walter, D., Wagner, T., Hörmann, C., Sihler, H., Dix, B., Frieß, U., Platt, U., Martinsson, B. G., van Velthoven, P. F. J., Zahn, A., and Ebinghaus, R.: SO_2 and BrO observation in the plume of the Eyjafjallajökull volcano 2010: CARIBIC and GOME-2 retrievals, Atmos. Chem. Phys., 11, 2973–2989, doi:10.5194/acp-11-2973-2011, 2011. 4231

Hönninger, G., Leser, H., Sebastian, O., and Platt, U.: Ground-based measurements of halogen oxides at the Hudson Bay by active longpath DOAS and passive MAX-DOAS, Geophys. Res. Lett., 31, L04111, doi:10.1029/2003GL018982, 2004a. 4231

Hönninger, G., Leser, H., Sebastian, O., and Platt, U.: Ground-based measurements of halogen oxides at the Hudson Bay by active longpath DOAS and passive MAX-DOAS, Geophys. Res. Lett., 31, L04111, doi:10.1029/2003GL018982, 2004b. 4232

Huijnen, V., Eskes, H. J., Poupkou, A., Elbern, H., Boersma, K. F., Foret, G., Sofiev, M., Valdebenito, A., Flemming, J., Stein, O., Gross, A., Robertson, L., D'Isidoro, M., Kioutsioukis, I., Friese, E., Amstrup, B., Bergstrom, R., Strunk, A., Vira, J., Zyryanov, D., Maurizi, A., Melas, D., Peuch, V.-H., and Zerefos, C.: Comparison of OMI NO_2 tropospheric columns with an ensemble of global and European regional air quality models, Atmos. Chem. Phys., 10, 3273–3296, doi:10.5194/acp-10-3273-2010, 2010. 4206

Jähne, B.: Digital Image Processing, Springer, 306–312, 2005. 4209

Kern, C., Sihler, H., Vogel, L., Rivera, C., Herrera, M., and Platt, U.: Halogen oxide measurements at Masaya Volcano, Nicaragua using active long path differential optical absorption spectroscopy, B. Volcanol., 71, 659–670, doi:10.1007/s00445-008-0252-8, 2009. 4232

Kern, C., Deutschmann, T., Vogel, L., Woehrbach, M., Wagner, T., and Platt, U.: Radiative transfer corrections for accurate spectroscopic measurements of volcanic gas emissions, B. Volcanol., 72, 233–247, doi:10.1007/s00445-009-0313-7, 2010. 4198

Kraus, S. G.: DOASIS, a Framework Design for DOAS, Ph.D. thesis, University of Mannheim, available at: http://www.iup.uni-heidelberg.de/institut/forschung/groups/atmosphere/software (last access: June 2012), 2006. 4202, 4203

AMTD
5, 4195–4247, 2012

Kurucz, R. L.: High resolution irradiance spectrum from 300 to 1000 nm, in: AFRL Transmission Meeting, AFRL Transmission Meeting, Lexington, Mass, available at: http://kurucz.harvard.edu/sun.html (last access: June 2011), 2005. 4203

Lehmann, T.: Improving the sensitivity of spectroscopic measurements of atmospheric trace gases by modern signal processing algorithms, in preparation, Ph.D. thesis, IUP, University Heidelberg, 2012. 4203

Leser, H., Honninger, G., and Platt, U.: MAX-DOAS measurements of BrO and NO_2 in the marine boundary layer, Geophys. Res. Lett., 30, 1537, doi:10.1029/2002GL015811, 2003. 4231

Liao, J., Sihler, H., Huey, L. G., Neuman, J. A., Tanner, D. J., Friess, U., Platt, U., Flocke, F. M., Orlando, J. J., Shepson, P. B., Beine, H. J., Weinheimer, A. J., Sjostedt, S. J., Nowak, J. B., Knapp, D. J., Staebler, R. M., Zheng, W., Sander, R., Hall, S. R., and Ullmann, K.: A comparison of Arctic BrO measurements by chemical ionization mass spectrometry and long path-differential optical absorption spectroscopy, J. Geophys. Res.-Atmos., 116, D00R02, doi:10.1029/2010JD014788, 2011. 4232

Mahajan, A. S., Plane, J. M. C., Oetjen, H., Mendes, L., Saunders, R. W., Saiz-Lopez, A., Jones, C. E., Carpenter, L. J., and McFiggans, G. B.: Measurement and modelling of tropospheric reactive halogen species over the tropical Atlantic Ocean, Atmos. Chem. Phys., 10, 4611–4624, doi:10.5194/acp-10-4611-2010, 2010. 4232

Marquard, L., Wagner, T., and Platt, U.: Improved air mass factor concepts for scattered radiation differential optical absorption spectroscopy of atmospheric species, J. Geophys. Res.-Atmos., 105, 1315–1327, doi:10.1029/1999JD900340, 2000. 4198

Matveev, V., Peleg, M., Rosen, D., Tov-Alper, D., Hebestreit, K., Stutz, J., Platt, U., Blake, D., and Luria, M.: Bromine oxide – ozone interaction over the Dead Sea, J. Geophys. Res.-Atmos., 106, 10375–10387, doi:10.1029/2000JD900611, 2001. 4232

Meller, R. and Moortgat, G.: Temperature dependence of the absorption cross sections of formaldehyde between 223 and 323 K in the wavelength range 225–375 nm, J. Geophys. Res.-Atmos., 105, 7089–7101, 2000. 4233

Merten, A., Tschritter, J., and Platt, U.: Design of differential optical absorption spectroscopy long-path telescopes based on fiber optics, Appl. Optics, 50, 738–754, 2011. 4198

Otten, C., Ferlemann, F., Platt, U., Wagner, T., and Pfeilsticker, K.: Groundbased DOAS UV/visible measurements at Kiruna (Sweden) during the SESAME winters 1993/94 and 1994/95, J. Atmos. Chem., 30, 141–162, doi:10.1023/A:1005810732347, 1998. 4231

AMTD
5, 4195–4247, 2012

Platt, U. and Stutz, J.: Differential Optical Absorption Spectroscopy: Principles and Application, Springer, doi:10.1007/978-3-540-75776-4, 2008. 4197, 4198

Platt, U., Marquard, L., Wagner, T., and Perner, D.: Corrections for zenith scattered light DOAS, Geophys. Res. Lett., 24, 1759–1762, doi:10.1029/97GL01693, 1997. 4204

Platt, U., Meinen, J., Pöhler, D., and Leisner, T.: Broadband Cavity Enhanced Differential Optical Absorption Spectroscopy (CE-DOAS) – applicability and corrections, Atmos. Meas. Tech., 2, 713–723, doi:10.5194/amt-2-713-2009, 2009. 4198

Poehler, D., Vogel, L., Friess, U., and Platt, U.: Observation of halogen species in the Amundsen Gulf, Arctic, by active long-path differential optical absorption spectroscopy, P. Natl. Acad. Sci. USA, 107, 6582–6587, doi:10.1073/pnas.0912231107, 2010. 4232

Puķīte, J., Kühl, S., Deutschmann, T., Platt, U., and Wagner, T.: Extending differential optical absorption spectroscopy for limb measurements in the UV, Atmos. Meas. Tech., 3, 631–653, doi:10.5194/amt-3-631-2010, 2010. 4198

Richter, A., Wittrock, F., Eisinger, M., and Burrows, J.: GOME observations of tropospheric BrO in northern hemispheric spring and summer 1997, Geophys. Res. Lett., 25, 2683–2686, doi:10.1029/98GL52016, 1998. 4231

Richter, A., Eisinger, M., Ladstätter-Weißenmayer, A., and Burrows, J.: DOAS zenith sky observations: 2. Seasonal variation of BrO over Bremen (53° N) 1994–1995, J. Atmos. Chem., 32, 83–99, doi:10.1023/A:1006077725894, 1999. 4231

Richter, A., Wittrock, F., Ladstätter-Weißenmayer, A., and Burrows, J. P.: GOME measurements of stratospheric and tropospheric BrO, Adv. Space Res., 29, 1667–1672, doi:10.1016/S0273-1177(02)00123-0, 2002. 4231

Roscoe, H. K., Fish, D. J., and Jones, R. L.: Interpolation errors in UV-visible spectroscopy for stratospheric sensing: implications for sensitivity, spectral resolution, and spectral range, Appl. Optics, 35, 427–432, doi:10.1364/AO.35.000427, 1996. 4204

Saiz-Lopez, A., Plane, J., and Shillito, J.: Bromine oxide in the mid-latitude marine boundary layer, Geophys. Res. Lett., 31, L03111, doi:10.1029/2003GL018956, 2004. 4232

Salawitch, R. J., Canty, T., Kurosu, T., Chance, K., and Jacob, D. J.: A new interpretation of total column BrO during Arctic spring, Geophys. Res. Lett., 37, L21805, doi:10.1029/2010GL043798, 2010. 4231

Stutz, J. and Platt, U.: Numerical analysis and estimation of the statistical error of differential optical absorption spectroscopy measurements with least-squares methods, Appl. Optics, 35, 6041–6053, doi:10.1364/AO.35.006041, 1996. 4209, 4212, 4217, 4219

AMTD

5, 4195–4247, 2012

Stutz, J., Thomas, J. L., Hurlock, S. C., Schneider, M., von Glasow, R., Piot, M., Gorham, K., Burkhart, J. F., Ziemba, L., Dibb, J. E., and Lefer, B. L.: Longpath DOAS observations of surface BrO at Summit, Greenland, Atmos. Chem. Phys., 11, 9899–9910, doi:10.5194/acp-11-9899-2011, 2011. 4232

Theys, N., Van Roozendael, M., Hendrick, F., Fayt, C., Hermans, C., Baray, J.-L., Goutail, F., Pommereau, J.-P., and De Mazière, M.: Retrieval of stratospheric and tropospheric BrO columns from multi-axis DOAS measurements at Reunion Island (21° S, 56° E), Atmos. Chem. Phys., 7, 4733–4749, doi:10.5194/acp-7-4733-2007, 2007. 4199, 4211

Theys, N., Roozendael, M. V., Dils, B., Hendrick, F., Hao, N., and Mazière, M. D.: First satellite detection of volcanic bromine monoxide emission after the Kasatochi eruption, Geophys. Res. Lett., 36, L03809, doi:10.1029/2008GL036552, 2009. 4231

Tuckermann, M., Ackermann, R., Golz, C., Lorenzen-Schmidt, H., Senne, T., Stutz, J., Trost, B., Unold, W., and Platt, U.: DOAS-observation of halogen radical-catalysed arctic boundary layer ozone destruction during the ARCTOC-campaigns 1995 and 1996 in Ny-Alesund, Spitsbergen, European-Geophysical-Society Symposium on Arctic Tropospheric Chemistry, The Hague, Netherlands, 6–10 May 996, Tellus B, 49, 533–555, doi:10.1034/j.1600-0889.49.issue5.9.x, 1997. 4232

Valks, P., Loyola, D., Hao, N., and Rix, M.: Algorithm Theoretical Basis Document for GOME-2 Total Column Products of Ozone, Minor Trace Gases, and Cloud Properties, Tech. rep., Deutsches Zentrum für Luft und Raumfahrt, Oberpfaffenhofen, Germany, 2009. 4231

Vandaele, A., Hermans, C., Simon, P., Carleer, M., Colin, R., and Fally, S.: Measurements of the NO_2 absorption cross-section from 42 000 cm^{-1} to 10 000 cm^{-1} (238–1000 nm) at 220 K and 294 K, J. Quant. Spectrosc. Ra., 59, 171–184, doi:10.1016/S0022-4073(97)00168-4, 1998. 4233

Vandaele, A., Hermans, C., and Fally, S.: Fourier transform measurements of SO_2 absorption cross sections: II. Temperature dependence in the 29 000–44 000 cm^{-1} (227–345 nm) region, J. Quant. Spectrosc. Ra., 110, 2115–2126, doi:10.1016/j.jqsrt.2009.05.006, 2009. 4233

Vogel, L.: Volcanic Plumes: Evaluation of Spectroscopic Measurements, Early Detection and Bromine Chemistry, Ph.D. thesis, Combined Faculties for the Natural Sciences and for Mathematics, Ruperto Carola University of Heidelberg, Germany, 2011. 4206, 4216, 4219

von Glasow, R.: Atmospheric chemistry in volcanic plumes, P. Natl. Acad. Sci. USA, 107, 6594–6599, doi:10.1073/pnas.0913164107, 2010. 4206

AMTD
5, 4195–4247, 2012

Wagner, T. and Platt, U.: Satellite mapping of enhanced BrO concentrations in the troposphere, Nature, 395, 486–490, doi:10.1038/26723, 1998. 4231

Wagner, T., Chance, K., Frieß, U., Gil, M., Goutail, F., Hönninger, G., Johnston, P., Karlsen-Tørnkvist, K., Kostadinov, I., Leser, H., Petritoli, A., Richter, A., Van Roozendael, M., and Platt, U.: Correction of the ring effect and I_0 effect for DOAS observations of scattered sunlight, ESA Technical Report, 2002. 4204

Wagner, T., Ibrahim, O., Sinreich, R., Frieß, U., von Glasow, R., and Platt, U.: Enhanced tropospheric BrO over Antarctic sea ice in mid winter observed by MAX-DOAS on board the research vessel Polarstern, Atmos. Chem. Phys., 7, 3129–3142, doi:10.5194/acp-7-3129-2007, 2007. 4231

Wagner, T., Beirle, S., and Deutschmann, T.: Three-dimensional simulation of the Ring effect in observations of scattered sun light using Monte Carlo radiative transfer models, Atmos. Meas. Tech., 2, 113–124, doi:10.5194/amt-2-113-2009, 2009. 4198

Wahner, A., Ravishankara, A. R., Sander, S. P., and Friedl, R. R.: Absorption cross-section of BrO between 312 and 385 nm at 298 and 223 K, Chem. Phys. Lett., 152, 507–512, 1988. 4205

Wenig, M., Jähne, B., and Platt, U.: Operator representation as a new differential optical absorption spectroscopy formalism, Appl. Optics, 44, 3246–3253, 2005. 4204

Wilmouth, D. M., Hanisco, T. F., Donahue, N. M., and Anderson, J. G.: Fourier transform ultraviolet spectroscopy of the $A^2\Pi_{3/2} \leftarrow X^2\Pi_{3/2}$ transition of BrO, RID A-2329-2008, J. Phys. Chem. A, 103, 8935–8945, doi:10.1021/jp991651o, 1999. 4205

AMTD
5, 4195–4247, 2012

Table 1. Selection of published DOAS measurements of BrO and the respective retrieval wavelength intervals used for the DOAS evaluation. The list is ordered by ascending lower wavelength limit and type of measurement (ground-based and airborne in the upper part, satellite instruments in the bottom part). The index number is given for orientation and further reference in later figures. In general, the list indicates the broad range of wavelength intervals applied.

Index	Lower limit [nm]	Upper limit [nm]	Type of measurement	Reference
1	310.9	377.8	MAX-DOAS, volc. plume	Boichu et al. (2011)
2	320	360	MAX-DOAS, volc. plume	Bobrowski and Platt (2007)
3	324	354	Airborne, volc. plume	Heue et al. (2011)
4	330	373.6	Airborne, volc. plume	Bani et al. (2009)
5	332	352	MAX-DOAS, volc. plume	Bobrowski and Platt (2007)
6	335.3	358.9	MAX-DOAS, Arctic	Wagner et al. (2007)
7	344.7	359	Zenith sky	Richter et al. (1999)
8	346	358	Zenith sky	Otten et al. (1998)
9	346	359	Zenith sky	Aliwell et al. (2002)
9	346	359	MAX-DOAS, Arctic	Hönninger et al. (2004b)
9	346	359	MAX-DOAS, volc. plume	Bobrowski and Platt (2007)
10	346.5	359.2	MAX-DOAS, m.b.l.[c]	Leser et al. (2003)
11	319	347.5	OMI	Salawitch et al. (2010)
12	336	347	SCIAMACHY	Afe et al. (2004)
12	336	347	GOME-2	Begoin et al. (2010)
13	336	351.1	GOME-2	Valks et al. (2009)
14	336	351.5	SCIAMACHY	De Smedt et al. (2004)
15	336	352	GOME-2	Theys et al. (2009)
16	336	360	GOME-2	Heue et al. (2011)
17	344.5	359	OMI	Chance (1998)
18	344.7	359	GOME	Richter et al. (1998)
19	345	359	GOME	Richter et al. (2002)
19	345	359	OMI	Chance (2002)
20	345	359.5	GOME	Wagner and Platt (1998)
21	346	359	GOME	Hegels et al. (1998)

AMTD
5, 4195–4247, 2012

Table 1. Continued.

Index	Lower limit [nm]	Upper limit [nm]	Type of measurement	Reference
22	308	341	LP-DOAS, Arctic	Poehler et al. (2010)
23	310	340	LP-DOAS, Arctic	Tuckermann et al. (1997)
24	312	357	LP-DOAS, Arctic	Hönninger et al. (2004a)
25	315.5	348	LP-DOAS, Arctic	Liao et al. (2011)
26	317	358	LP-DOAS, m.b.l.[c]	Saiz-Lopez et al. (2004)
27	324	357	LP-DOAS, m.b.l.[c]	Mahajan et al. (2010)
28	327	347	LP-DOAS, salt lake	Matveev et al. (2001)
29	329[a]	347[a]	LP-DOAS, salt lake	Hebestreit et al. (1999)
30	331	357	LP-DOAS, volc. plume	Kern et al. (2009)
31	332[b]	351[b]	LP-DOAS, Arctic	Stutz et al. (2011)

[a] derived from Hebestreit et al. (1999), Fig. 1;
[b] 338.7–342.3 nm and 346.1–347.4 nm excluded;
[c] marine boundary layer.

AMTD
5, 4195–4247, 2012

Table 2. SCDs used in the construction of synthetic spectra for the two different measurement scenarios. The zenith-sky DOAS scenario corresponds to the composition of SCDs typical for Zenith-sky measurements of stratospheric BrO at mid-latitudes. It reproduces the settings in (Aliwell et al., 2002). The second scenario, volcanic plumes, applies typical SCDs of trace gases for MAX-DOAS measurements of BrO in tropospheric volcanic plumes.

Trace gas	Temperature [K]	Reference cross-section	Zenith-sky DOAS [molec cm^{-2}]	Volcanic plumes [molec cm^{-2}]
BrO	298 K	Fleischmann et al. (2004)	1.5×10^{14}	1.5×10^{14}
O_3	221 K	Burrows et al. (1999)	8×10^{19}	0
O_3	241 K	Burrows et al. (1999)	2×10^{19}	0
O_3	273 K	Burrows et al. (1999)	0	1×10^{18}
NO_2	220 K	Vandaele et al. (1998)	5×10^{16}	0
NO_2	294 K	Vandaele et al. (1998)	0	5×10^{16}
SO_2	298 K	Hermans et al. (2009); Vandaele et al. (2009)	0	1×10^{18}
HCHO	298 K	Meller and Moortgat (2000)	0	3×10^{16}

AMTD
5, 4195–4247, 2012

Table 3. Differential optical densities of trace gases at SCDs applied in the measurement scenarios of BrO in volcanic plumes. The differential optical densities are calculated by taking the peak to peak value of a high pass filtered absorption cross sections multiplied with the respective SCD in a 5 nm wavelength interval. The 325 nm and 350 nm wavelengths were chosen to indicate approximate optical densities in the lower and higher wavelength ranges. The strongest absorption band of BrO is situated at ≈338 nm.

Center of wavelength interval	Optical density [10^{-3}]				
[nm]	BrO	SO_2	O_3	NO_2	HCHO
325	0.7	6.2	5.0	0.7	1.0
338	1.2	0.1	1.2	2.0	0.7
350	0.3	0.1	0.1	3.5	0.2

AMTD
5, 4195–4247, 2012

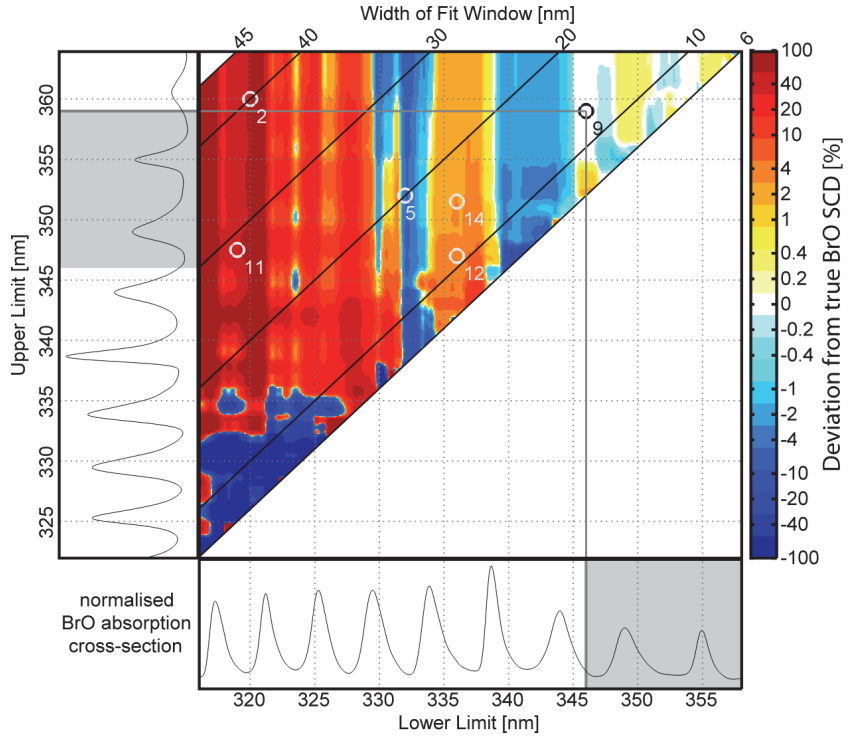

Fig. 1. Wavelength interval mapping of a synthetic spectrum. Zenith-sky measurements of stratospheric BrO (Table 2) are simulated with a true BrO SCD of 1.5×10^{14} molec cm^{-2}. The retrieval applies I_0 corrected RCSs. The abscissa-axis shows the lower wavelength limit of the retrieval wavelength interval, the ordinate-axis the upper wavelength limit. Deviations from the true BrO SCD are displayed colour-coded on logarithmic colour-scale. The circles mark selected retrieval wavelength intervals in the literature, which are referenced by the given number in Table 1. The highlighted wavelength interval denotes the optimal retrieval wavelength interval found by Aliwell et al. (2002).

AMTD
5, 4195–4247, 2012

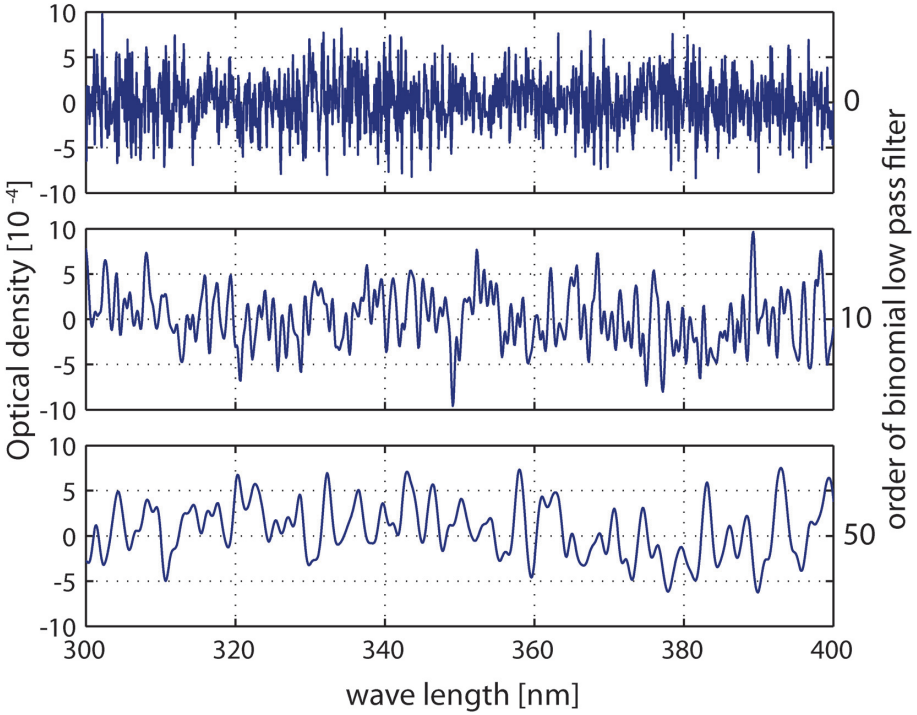

Fig. 2. Examples of different Gaussian noise spectra added to the logarithm of the synthetic spectrum. The broad band structures are introduced by a low pass filter using a binomial filter of 0 (top trace), 10 (center trace) and 50 (bottom trace) iterations, respectively. After low pass filtering, the noises were rescaled to the original standard deviation of amplitude of 3×10^{-4}.

AMTD
5, 4195–4247, 2012

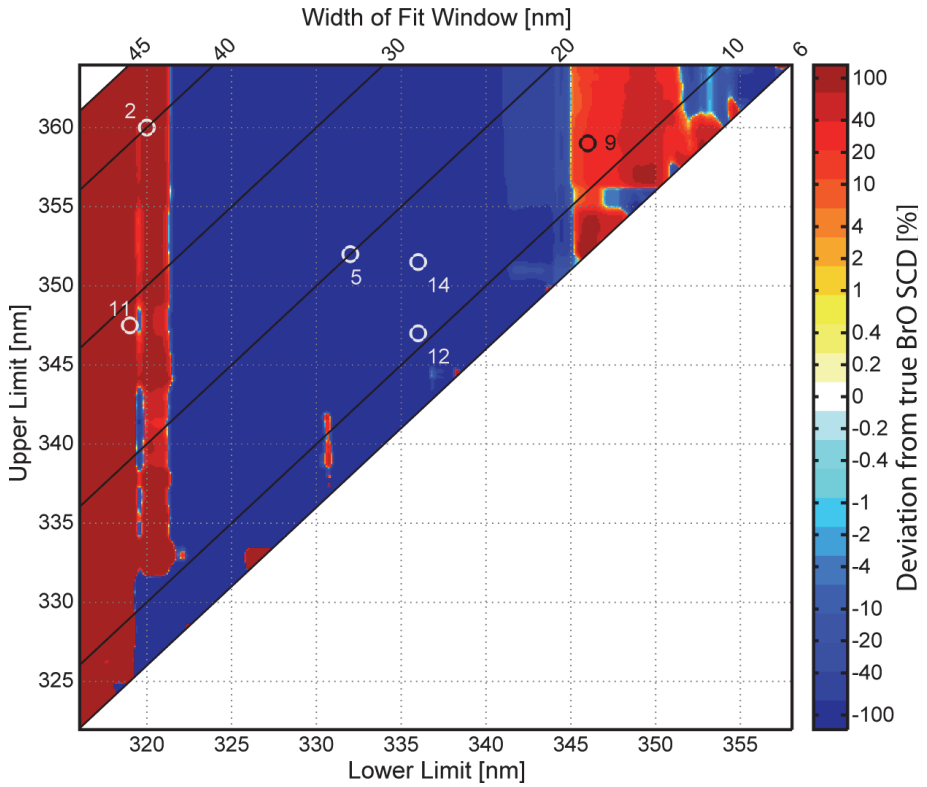

Fig. 3. Results from a retrieval wavelength mapping of a synthetic spectrum for measurement scenario zenith-sky DOAS with a true BrO SCD of 1.5×10^{14} molec cm^{-2}. The plot shows a retrieval map constructed with uncorrected RCSs used in the retrieval. Note that the color-code is on a logarithmic scale. Compared to the retrieval applying corrected RCSs (Fig. 1), highly erroneous values are retrieved. The numbers denote certain wavelength intervals shown in Table 1.

AMTD
5, 4195–4247, 2012

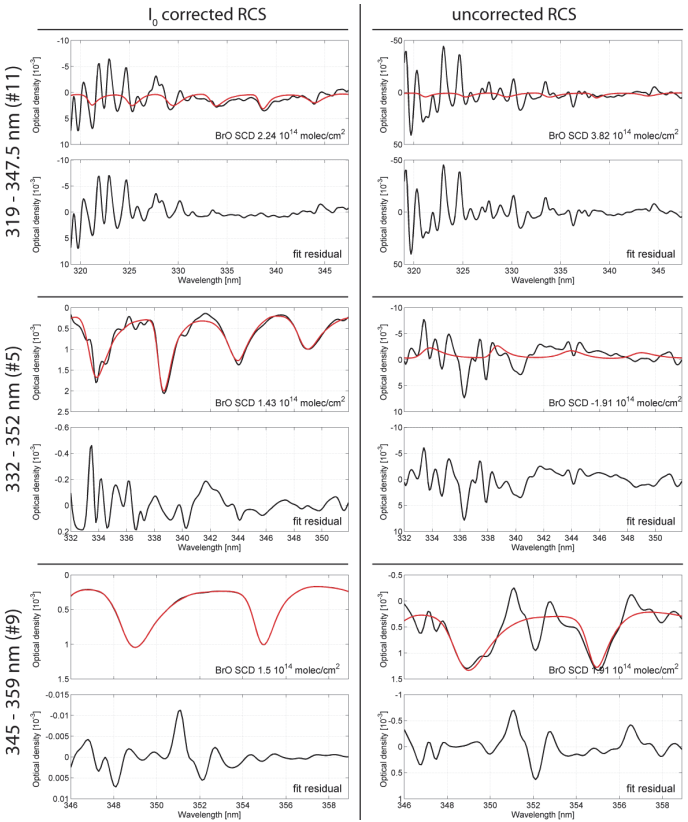

Fig. 4. Shown are fit results of the measurement scenario zenith-sky DOAS for three different wavelength intervals, corresponding to #11, #5 and #9 in Table 1. The fit of BrO RCS and the residuum are displayed. Left column: uncorrected RCSs; right column: I_0 corrected RCSs. Regardless which RCSs are used, a fit applying the longest wavelengths (346–359 nm) yields the most accurate results. At 346–359 nm, tests C1 and C2 on synthetic spectra in Aliwell et al. (2002) are reproduced.

AMTD
5, 4195–4247, 2012

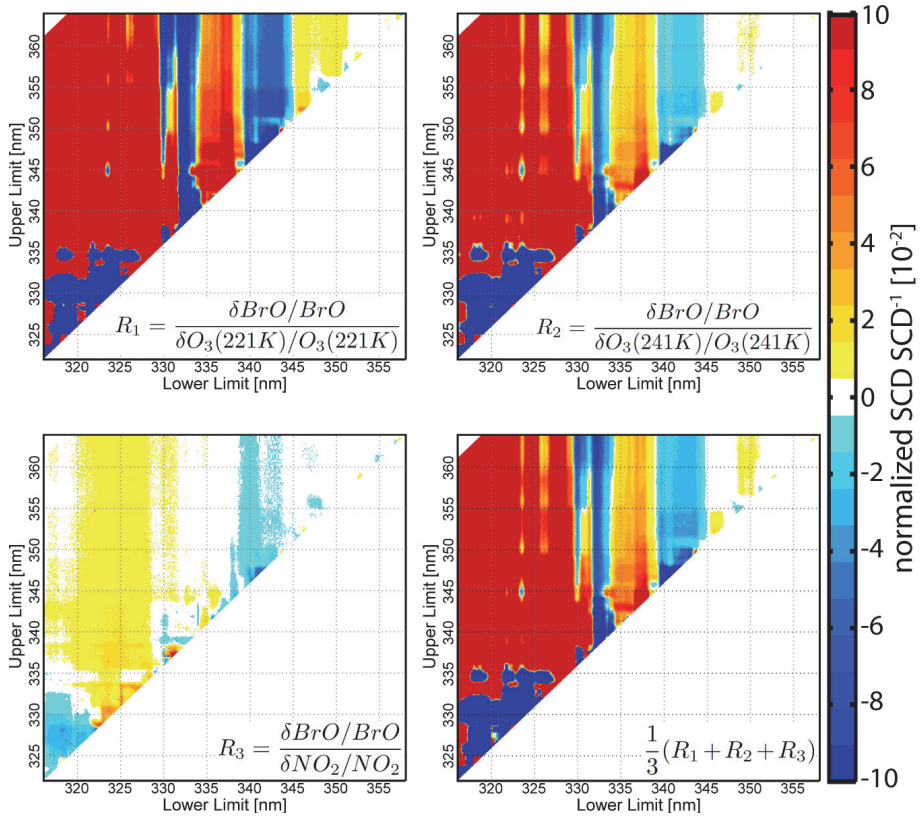

Fig. 5. Interference study for the zenith-Sky DOAS scenario: changes in BrO SCDs if potentially interfering absorbers are varied by 1 %. The color-code depicts relative changes of retrieved BrO SCD per relative change of absorber. At shorter wavelengths, clearly the strong O_3 absorptions are dominating (upper row), whereas the influence of NO_2 is negligible in comparison (lower left). The average of all relative changes is depicted in the lower right graph.

AMTD
5, 4195–4247, 2012

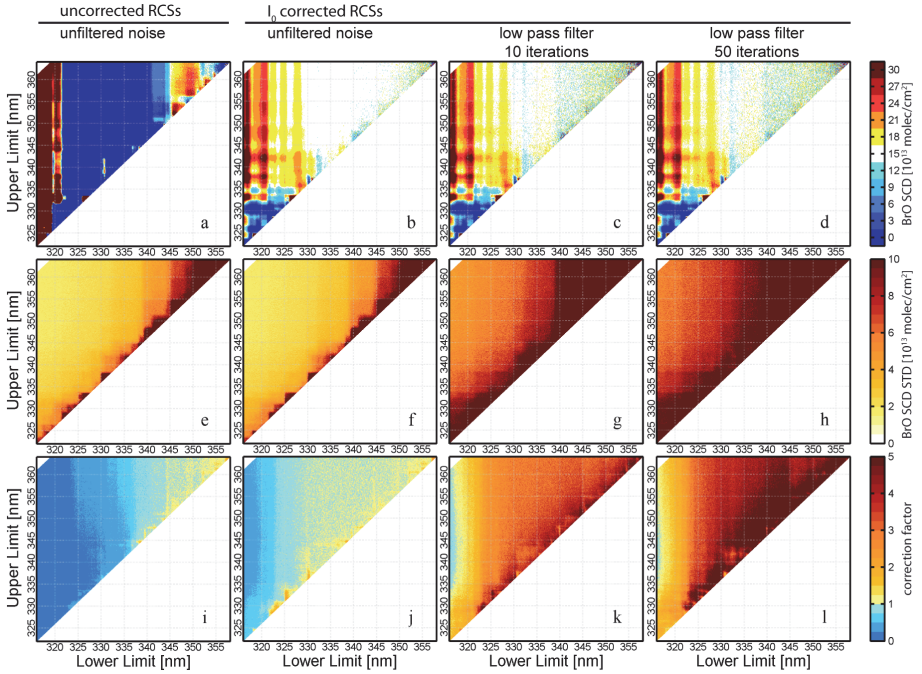

Fig. 6. Results from the statistical study on measurement scenario of zenith-sky DOAS. For information on noises applied to the synthetic spectra, the reader is referred to Sect. 3.3.3. The first column shows results for an uncorrected set of RCSs together with unfiltered noise. Second till fourth column depict results for I_0 corrected RCSs and different filtered noises. The rows (upper to lower) correspond to retrieved SCDs, standard deviation of results, and calculated correction factor to retrieve the standard deviation from the fitting error (top to bottom row, respectively).

AMTD
5, 4195–4247, 2012

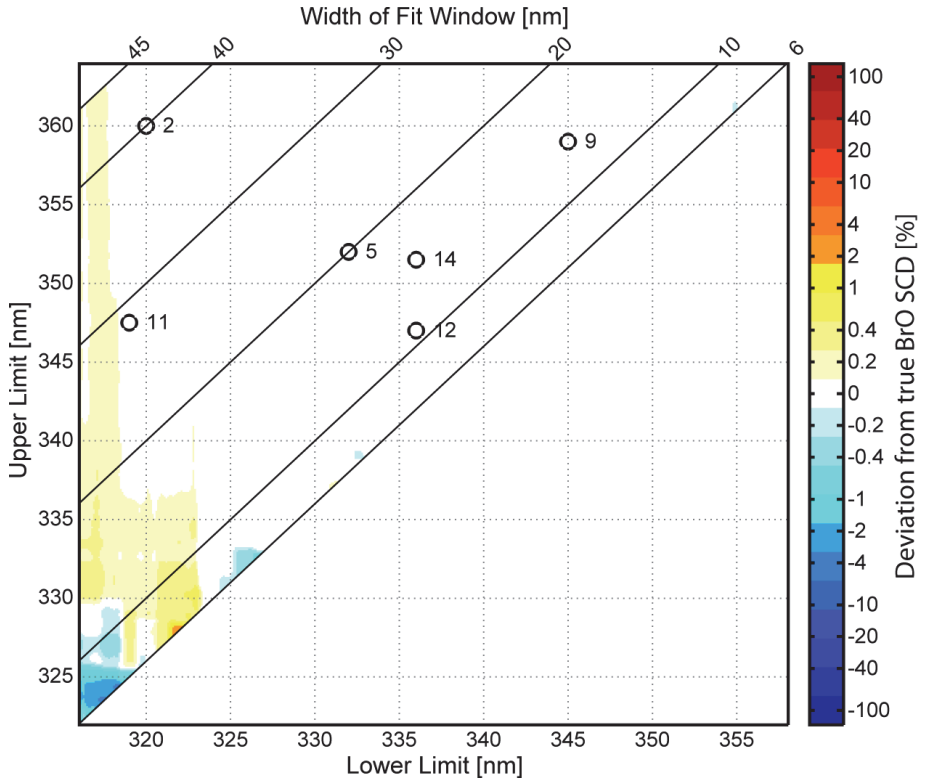

Fig. 7. Deviations from the true BrO SCD (1.5×10^{14} molec cm^{-2}) for the measurement scenario of BrO in volcanic plumes using I_0 corrected RCS. The retrievals only show minor structures if lower wavelengths are included in the fit. The numbers indicate the different retrieval ranges in Table 1.

AMTD
5, 4195–4247, 2012

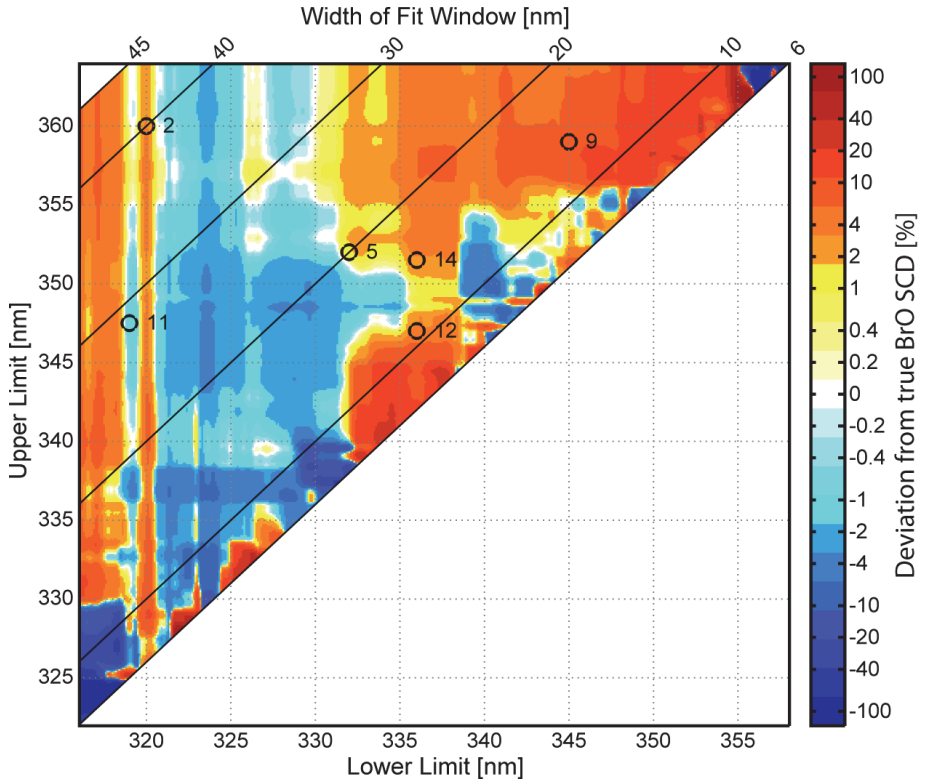

Fig. 8. Deviations from the true BrO SCDs with uncorrected RCSs in the measurement scenario of volcanic plumes. Over- or underestimation of the target BrO SCD of 1.5×10^{14} molec cm^{-2} is higher compared to I_0 corrected RCS (Fig. 7). Retrievals at longer wavelength ranges (>345 nm) systematically overestimate the BrO SCD. The index numbers denote selected wavelength intervals from Table 1.

AMTD
5, 4195–4247, 2012

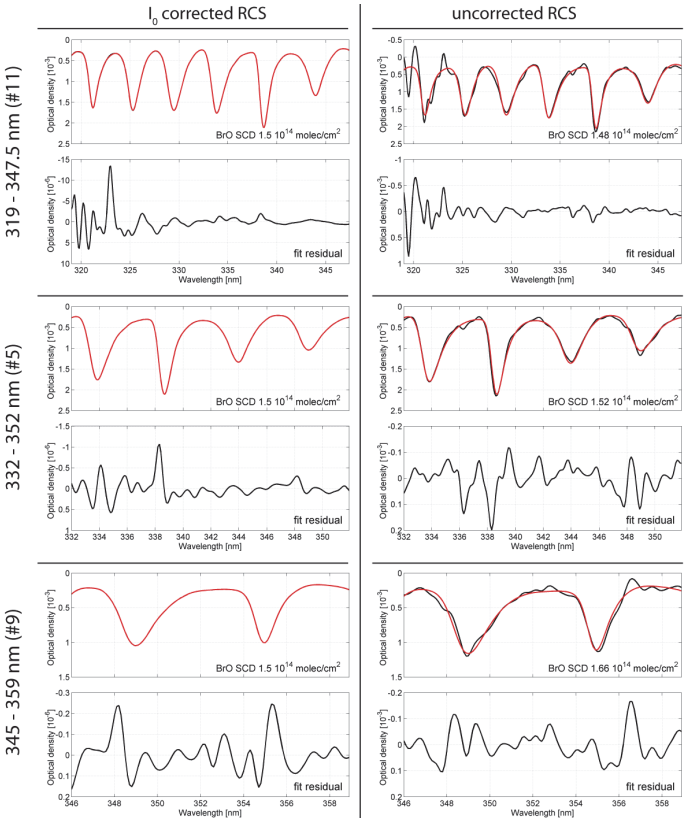

Fig. 9. Fit examples of selected wavelength intervals (# 11, #5, #9 in Table 1) for the scenario BrO in volcanic plumes: all wavelength intervals yield results with negligible residual structures for I_0 corrected RCSs. For fits applying uncorrected RCSs, the largest deviation is seen for the interval of 346–359 nm (#9) in contrast to the scenario of zenith-sky DOAS (Fig. 4). Please note that the optical density for the fit residual is given in units of 10^{-6} for I_0 corrected RCSs and in units of 10^{-3} for uncorrected RCSs.

AMTD
5, 4195–4247, 2012

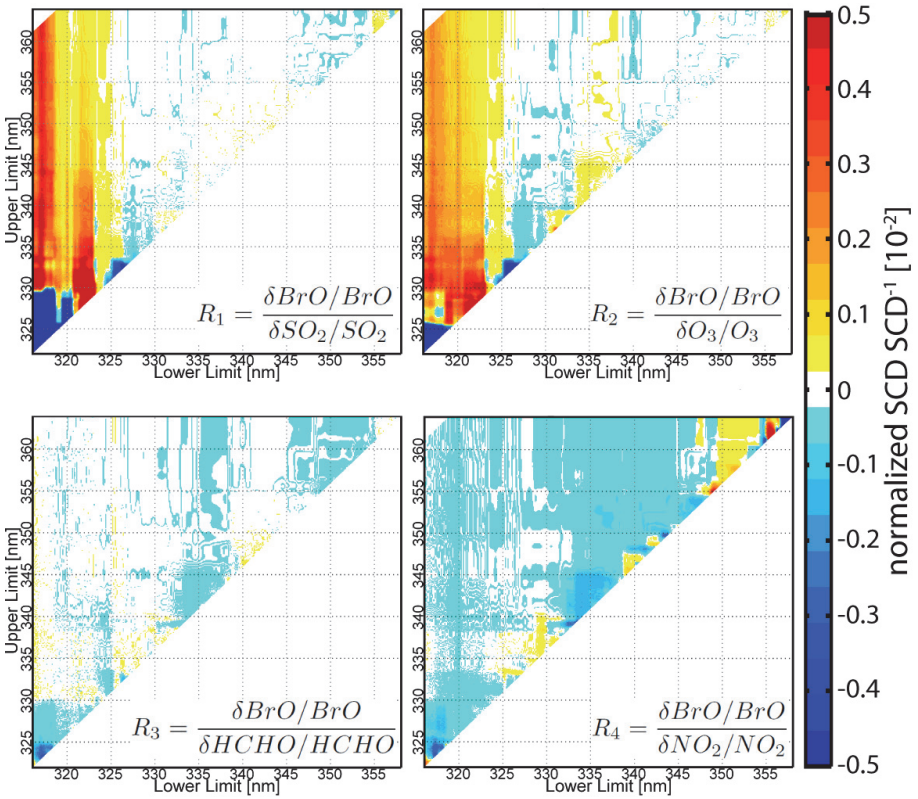

Fig. 10. The figures depicts the influence of varying absorber strength on the retrieval of BrO in volcanic plumes. Retrieval wavelength maps are constructed with varying absorber strengths by 10 %. The original I_0 corrected set of RCSs was used. Greatest deviations from the true BrO SCD occur where strong absorption features of SO_2 or O_3 are included (e.g. at evaluation ranges including wavelengths ≤323 nm). While these effects correlated to the BrO SCDs, NO_2 and HCHO mostly anti-correlate with BrO, with NO_2 absorptions showing greater influence.

AMTD
5, 4195–4247, 2012

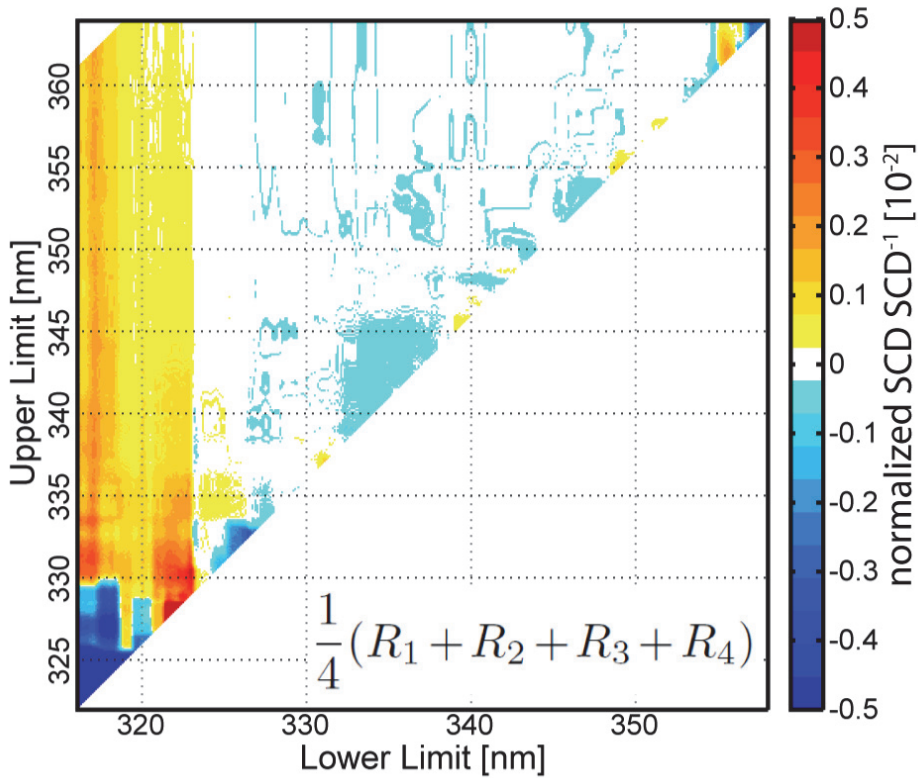

Fig. 11. The figure depicts the average of interferences of other trace gases with the BrO retrieval (Fig. 7). Wavelength evaluation ranges with a lower limit <325 are dominated by O_3 and SO_2 features, where as the other wavelength ranges may be influenced mainly by NO_2 and HCHO.

AMTD
5, 4195–4247, 2012

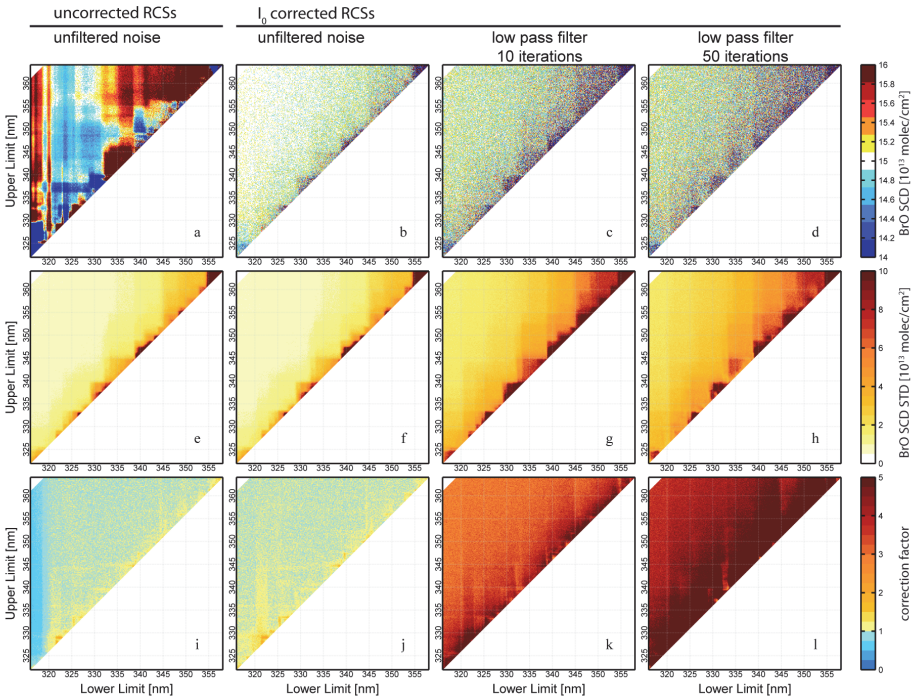

Fig. 12. The graph depicts results of the the statistical study for the scenario of measuring BrO in volcanic plumes. Different types of noise spectra were added to the logarithm of the synthetic spectra (see Sect. 3.3.3). The first column shows results for unfiltered noise and an uncorrected set of RCSs applied in the fit. In the second, third and fourth column, results are plotted for I_0 corrected RCSs applied to synthetic spectra with unfiltered noise and low pass filtered noise. The mean BrO SCDs retrieved are shown in the top row, the middle row gives the standard deviation of SCDs and the bottom row the calculated error correction coefficient.

AMTD
5, 4195–4247, 2012

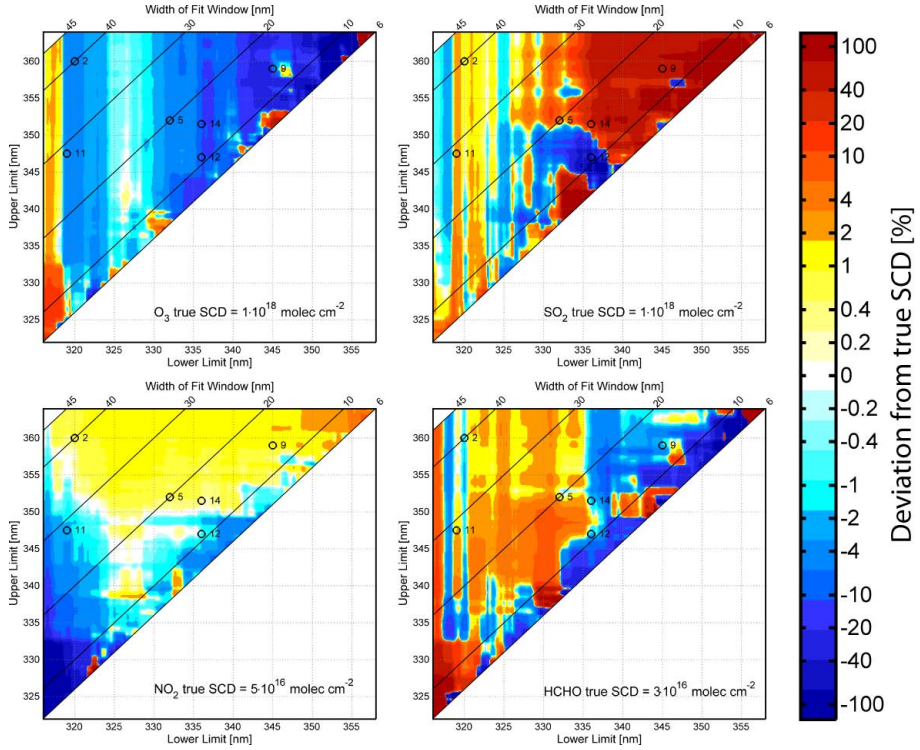

Fig. 13. Deviations from the true SCDs of other trace gases than BrO in test I of measurement scenario volcanic plumes using uncorrected RCSs. The respective true SCD is indicated in white (0 % deviation), over- and underestimation in red and blue colours.

AMTD
5, 4195–4247, 2012